FIRE-RES

Innovative technologies & socio-ecological-economic solutions for fire resilient territories in Europe

D5.6 IA 5.5 brief: Earth Observation data collection to support decision making

www.fire-res.eu

fire-res@ctfc.cat

Project Acronym: FIRE-RES

Project name: Innovative technologies and socio-ecological-economic solutions for fire resilient territories in Europe

Call ID: H2020-LC-GD-1-1-2020 (Preventing and fighting extreme wildfires with the integration and demonstration of innovative means)

Work Package: 5

Task Number: 5.2

Lead beneficiary: Spire Global Luxembourg s.a.r.l.

Contributing beneficiary(ies): Institut Cartogràfic i Geològic de Catalunya (ICGC)

This document was produced under the terms and conditions of Grant Agreement No. 101037419 of the European Commission. It does not necessarily reflect the view of the European Union and in no way anticipates the Commission's future policy in this area.

D5.6 IA 5.5 BRIEF: EARTH OBSERVATION DATA COLLECTION TO SUPPORT DECISION MAKING

Publication

Publication date: 29/11/2024

Authors: Gerald van der Grijn (Spire), Arnau Ferràndiz Ensesa (ICGC)

Abstract: This report, prepared collaboratively by Spire and ICGC, presents key contributions to the FIRE-RES project, focusing on two critical aspects of wildfire resilience: atmospheric and vegetation data collection through satellite remote sensing techniques. Part 1 leverages Spire's satellite-based Radio Occultation (RO) data to collect atmospheric profiles to improve numerical weather predictions, especially under extreme wildfire event (EWE) conditions. The data assimilation methods applied significantly increase forecast accuracy across key atmospheric variables essential for fire risk assessment. Part 2, led by ICGC, explores advanced vegetation data collection techniques, combining satellite remote sensing and AI-driven time-series analysis to estimate fire severity, biomass consumption, CO_2 emissions, and post-fire recovery. Together, these methodologies support a holistic approach to EWE preparedness and response across Europe.

Key words: Extreme Wildfire Events, Satellite Remote Sensing, Earth Observations, Numerical Weather Prediction (NWP), Vegetation Characterization

Quote as: van der Grijn, G., Ferràndiz Ensesa, A., (2024). FIRE-RES Earth Observation Data Collection to Support Decision-Making. Deliverable D5.6 FIRE-RES project. 44 pages. DOI: 10.5281/zenodo.14188148

DOI: 10.5281/zenodo.14188148

Dissemination level

[X] PU- Public: must be available in the website

[ ] CO- Confidential: Only for members of the Consortium and the Commission Services

[ ] CI – Classified: As referred in to Commission Decision 2001/844/EC

Document history

Edition	Date	Status	Author
Version 1	31/10/2024	Draft	Gerald van der Grijn (Spire), Arnau Ferràndiz Ensesa (ICGC)
Version 2	5/11/2024	Review	Miguel Mendes (TSYLVA)
Final version	19/11/2024	Revisions of reviewers incorporated.	Gerald van der Grijn (Spire), Arnau Ferràndiz Ensesa (ICGC)

Table of contents

List of acronyms

4DVar - Four-Dimensional Variational Assimilation

4DEnVar – Four-Dimensional Ensemble Variational Data Assimilation

AI – Artificial Intelligence

CGMS – Coordination Group for Meteorological Satellites

COSMIC – Constellation Observing System for Meteorology, Ionosphere, and Climate

CREAF – Centre de Recerca Ecològica i Aplicacions Forestals

dNBR – Differenced Normalised Burn Ratio

ECMWF – European Centre for Medium-Range Weather Forecasts

EO – Earth Observation

ESA – European Space Agency

EWE – Extreme Wildfire Event

FSOI – Forecast Sensitivity to Observation Impact

GFS – Global Forecast System

GLONASS – GLObal Navigational Satellite System (Russia)

GNSS-RO – Global Navigation Satellite System Radio Occultation

GPS – Global Positioning System (USA)

GRAS – GNSS Receiver for Atmospheric Sounding

IA – Innovation Action

ICGC – Institut Cartogràfic i Geològic de Catalunya

IROWG – International Radio Occultation Working Group

ISS – Integrative Software System

LEO – Low Earth Orbiting

LIDAR – Laser Imaging Detection and Ranging

NBAM – NCEP Bending Angle Model

NCEP – National Center for Environmental Prediction

NDVI – Normalized Difference Vegetation Index

NIR – Near Infrared

NOAA – National Oceanic and Atmospheric Administration

NOCCS – Number of Occultations

NWP – Numerical Weather Prediction

OSE – Observation System Experiment

POD – Precise Orbit Determination

RO – Radio Occultation

RMSE/D – Root Mean Square Error/Difference

SNR – Signal-to-Noise Ratio

SOFD – Spire Operational Forecast Deterministic

SWIR – Short-wave Infrared

TRL – Technology Readiness Level

UFS – Unified Forecast System

VGI – Vegetation Growth Index

WP – Work Package

List of figures

List of tables

1. INTRODUCTION

Wildfires have increasingly posed significant environmental, social, and economic challenges across Europe. Recent Extreme Wildfire Events (EWEs) have highlighted the need for comprehensive, data-driven approaches to wildfire prediction, prevention, and response. The FIRE-RES project, funded under the European Commission's Horizon 2020 initiative, aims to address these challenges by developing innovative technologies and strategies to enhance fire resilience. This report, prepared collaboratively by Spire and the Institut Cartogràfic i Geològic de Catalunya (ICGC), focuses on two essential components of this project: atmospheric and vegetation data collection. Through advanced satellite remote sensing techniques, each aspect contributes critical insights into both the environmental conditions that drive wildfires and the impacts of these events on the ecosystem.

1.1 The Role of Atmospheric Data in Fire Prediction

The atmosphere plays a critical role in the development, spread, and intensity of wildfires. Conditions such as temperature, humidity, wind speed, and pressure influence the likelihood and behaviour of fires. Therefore, understanding and forecasting atmospheric conditions is crucial for wildfire preparedness and response. Satellite-based Radio Occultation (RO), a technique that collects atmospheric data by observing the refraction of radio signals as they pass through the atmosphere, offers high-resolution, unbiased profiles of these essential parameters.

Spire, leveraging its constellation of nanosatellites, has implemented RO technology to enhance atmospheric profiling. These satellites collect RO data from multiple Global Navigation Satellite System (GNSS) constellations, such as the Global Positioning System (GPS) and Galileo, delivering global atmospheric profiles with high vertical resolution. The data collected is assimilated into Spire's weather prediction models to create detailed forecasts. This process includes refining initial conditions for Numerical Weather Prediction (NWP) models, improving forecast accuracy, and enabling more precise predictions of weather variables, such as temperature, wind, and humidity that directly influence wildfire risks.

The RO data's ability to produce unbiased, globally distributed profiles has proven indispensable for enhancing weather model performance, especially in remote and data-scarce regions. This is achieved by integrating bending angle measurements into data assimilation frameworks, which optimize the forecasts by reconciling observational data with model outputs. Additionally, the high vertical resolution provided by RO technology allows Spire to monitor conditions across the full atmospheric vertical column, from the lower troposphere up to the upper stratosphere. This capability supports early detection and real-time tracking of weather conditions that can exacerbate fire hazards, such as prolonged dry spells or high wind speeds, which fuel fire spread.

1.2 Advanced Vegetation Data Collection for Wildfire Impact Assessment

Beyond atmospheric conditions, the state of vegetation plays a pivotal role in wildfire dynamics. Fuel characteristics, such as biomass density and moisture levels, are directly related to fire intensity and spread. Accurate assessments of vegetation health, biomass distribution, and fuel conditions are essential for understanding the full scope of wildfire impact and for planning effective recovery measures. In Part 2 of this report, ICGC applies satellite remote sensing, coupled with Artificial Intelligence (AI) methodologies, to monitor vegetation and analyse post-fire recovery in affected areas.

ICGC's work in this report centres around high-resolution vegetation monitoring, utilizing multi-temporal satellite imagery to derive key vegetation indices such as the Normalized Difference Vegetation Index (NDVI) and the Vegetation Growth Index (VGI). By analysing time-series data from Sentinel-2 and other satellite sources, this approach enables an assessment of both pre- and post-fire vegetation dynamics. Estimations of biomass consumption and CO_2 emissions are derived by analysing the burn severity using indices like the differenced Normalized Burn Ratio (dNBR). This index allows for the identification of vegetation loss, providing an essential measure of the ecological impact of wildfires and the potential carbon release due to biomass consumption.

ICGC's integration of AI models further enhances vegetation monitoring by capturing trends and predicting future vegetation conditions based on historical data. These AI-driven analyses utilize time-series data to identify patterns in vegetation health, assess post-fire regrowth rates, and forecast future vegetation vulnerabilities under changing climate conditions. Together, these techniques provide a comprehensive understanding of vegetation's role in fire dynamics and recovery, supporting proactive fire management strategies.

1.3 Integrated Approach to Fire Resilience

The integration of atmospheric and vegetation data collection reflects a holistic approach to wildfire resilience. By combining Spire's atmospheric profiling capabilities with ICGC's advanced vegetation monitoring, the FIRE-RES project aims to create a comprehensive framework for wildfire management. This approach allows for more accurate fire risk assessments, timely decision-making, and improved resource allocation in response to evolving fire conditions.

Through real-time data assimilation and predictive modelling, this collaborative effort strengthens the ability of European stakeholders to prepare for and respond to EWEs. This data-driven approach, informed by both weather and vegetation conditions, not only supports immediate firefighting needs but also contributes to long-term strategies for

ecosystem restoration and climate adaptation. The methodologies presented in this report exemplify the innovative solutions that FIRE-RES brings to wildfire management, contributing to more resilient landscapes and communities across Europe.

2. ATMOSPHERIC DATA COLLECTION

Part 1 presents the outcomes of Subtask 5.2.2 within Work Package 5 (WP5) of the FIRE-RES project, specifically focused on leveraging Spire's atmospheric data to enhance wildfire resilience. By integrating satellite data with advanced forecasting models, we aim to provide actionable insights that support decision-making processes and enable more effective responses to Extreme Wildfire Events across Europe.

In the text, both GNSS-RO and RO are used interchangeably to refer to Global Navigation Satellite Systems Radio Occultation, a technique for capturing high-resolution atmospheric data essential to weather forecasting.

2.1 Background

Spire is a global provider of space-based data, analytics, and space services, offering unique datasets and powerful insights about Earth's weather and climate. Spire builds, owns, and operates a fully deployed satellite constellation that observes the Earth in real-time using radio frequency technology (Cappaert, 2018). Since its founding in 2012, Spire has deployed the world's largest constellation of multipurpose satellites with over 175 satellites launched into orbit and over 600 years of flight heritage. Spire additionally operates a network of more than 30 ground stations globally that enables the timely downlink and dissemination of data collected on-orbit to end users.

The collection of Global Navigation Satellite System (GNSS) radio occultation data is one of the primary purposes of Spire's constellation of satellites. GNSS radio occultation is an atmospheric remote sensing technique that utilizes L-band radio frequency transmissions from GNSS satellites in medium-earth-orbit and corresponding receivers' onboard satellites in low-earth-orbit. During a radio occultation (RO) sounding, the transmitted GNSS signal traverses the Earth's atmosphere where it undergoes a level of refraction dependent on the properties of the atmosphere. The primary variable of interest during a RO sounding is a vertical profile of the amount signal bending induced by the atmosphere, which is a product of more commonly understood atmospheric variables of temperature, pressure, and water vapor. The amount of bending induced by the atmosphere can be precisely estimated by measuring the GNSS signal change over the course of an RO sounding and carefully removing instrumental and geometrical effects. The GNSS-RO method has many advantages over other atmospheric remote sensing techniques including high vertical resolution, and minimal biases. Consequently, it has become one of the most important observations for improving numerical weather forecasting through data assimilation, ranking only behind microwave radiance and high spectral-resolution infrared data in operational impact (Cardinali & Healy, 2014). Additional characteristics of the RO technique such as long-term stability and self-calibration make it well suited to act as a climate benchmark (Lackner et al., 2011).

RO has a rich history of research and development that dates back to the early 1960s when scientists used radio links between Earth and the Mariner 3 and 4 spacecraft to study the atmospheric properties of Mars. GNSS-RO was demonstrated for remote sensing of the Earth's atmosphere for the first time by the GPS/MET instrument in 1995

(Rocken et al., 1997). Many additional publicly funded satellite missions collecting GNSS-RO have since followed including CHAMP, SAC-C, COSMIC-1, COSMIC-2, and MetOp A/B/C. The COSMIC-1 mission, launched in 2008, was particularly instrumental in demonstrating the potential value of RO data in the improvement of operational global weather forecasting. Numerous studies were able to quickly demonstrate the utility of COSMIC-1 data in improving global weather forecasts and hurricane forecast tracks (Anthes et al., 2008; Cucurull et al., 2010; Marshall et al, 2012). Furthermore, observation impact studies have using simulated RO data have shown that the impact of RO data on numerical weather prediction increases as the number of assimilated profiles is scaled upward with no saturation up to 128,000 profiles per day (Harnisch et al, 2013; Bauer et al., 2014). As of today (2024), this number is over 10 times greater than the total number of RO profiles available from publicly funded satellite missions.

2.2 GNSS-RO Data Collection

As of July 2024, Spire has launched over 90 satellites with the capability to collect GNSS signals for RO and other applications. Most of the GNSS-RO capable satellites that have been launched have adopted the 3U CubeSat form factor (Figure 1). The advantages of building and launching satellites with these small dimensions are well known and include lower engineering costs, easier access to space as secondary payloads on launch vehicles, and faster manufacturing time. Spire has miniaturized and advanced the capability beyond other RO receivers without reducing performance. Each Spire satellite that is currently in-orbit hosts multiple payloads onboard that can operate concurrently to deliver data to a diverse set of end users downstream.

Figure 1 Picture of Spire's 3U nanosatellite capable of collecting GNSS-RO measurements

As illustrated in Figure 1, each GNSS-RO capable satellite is equipped with one or two limb-facing "RO" antennas to collect GNSS signals that are occulted by the Earth's atmosphere. These GNSS signals are tracked using Spire's in-house designed and

manufactured STRATOS software-designed receiver. Since being introduced into orbit in 2016, the STRATOS receiver has undergone years of continuous iteration that has produced the unmatched ability to efficiently track GNSS signals at science-grade quality while optimizing size and power consumption.

Years of rapid development and in-house innovation have produced the latest version of Spire's RO payload that compares favourably with any other GNSS-RO payload in the world. A summary of Spire's receiver capabilities in comparison to COSMIC-2, currently the largest publicly funded RO mission, is provided in Table 1. Like the receiver flown for the COSMIC-2 mission, Spire performs open-loop tracking in order to consistently measure the signal down to the lowest layers of the troposphere, a region that has been historically difficult to track due to signal fading and dynamics, but crucial for Numerical Weather Prediction (NWP). However, the Spire receiver can collect approximately twice the number of profiles per satellite compared to COSMIC-2 due to its capability of tracking all major GNSS constellations (GPS, GLONASS, Beidou and Galileo). The one advantage where the COSMIC-2 receiver has over Spire's STRATOS is the received signal-to-noise ratio (SNR). This is a result of COSMIC-2's larger satellite dimensions, which allows for larger antenna size and gain. However, this does not necessarily translate to better measurement quality as described later in the deliverable.

Table 1 Comparison between Spire and COSMIC-2 receiver capabilities. COSMIC-2 values are taken from https://space.oscar.wmo.int/instruments/view/tgrs_cosmic_2

	Spire (STRATOS)	COSMIC-2
GNSS Constellations Tracked	GPS, GLONASS, Beidou, Galileo	GPS, GLONASS, Galileo (as of 2024)
Maximum number of occultations collected per 24 hours per receiver	2000	900
Power	< 6 W	65 W
Coverage	90° S – 90° N	45° S – 45° N
Tracking technique	Open-loop	Open-loop
Signal-to-noise Ratio (V/V)	600	2,500

2.2.1 GNSS-RO technology

Originally designed for positioning, navigation and timing purposes, electromagnetic signals transmitted from Global Navigation Satellite System (GNSS) constellations, such as GPS (USA), Galileo (Europe), GLONASS (Russia) and Beidou (China), are now being used for a variety of scientific and technological applications. One such application is the measurement of atmospheric properties through a technique called radio occultation. In a radio occultation, a signal transmitted from a GNSS satellite passes through the limb of the Earth's atmosphere, is delayed and bent due to refraction, and subsequently, received by a GNSS receiver in a low Earth orbit (LEO).

Figure 2 depicts an example of a setting radio occultation scenario where a GNSS signal descends through lower portions of the atmosphere over a short period of time. By precisely recording and analysing the signal phase and amplitude during the occultation event, vertical profiles of atmospheric properties, such as pressure, temperature and humidity from 0 to 60 km altitude, can be derived. Accurate retrievals of atmospheric profiles are made possible due to the stability of the GNSS signal frequency, which is essential to computing the bending and delay of the signal as it passes through the atmosphere. Past satellite missions have demonstrated that radio occultation measurements of the atmosphere are accurate and have an enormous impact on weather specification and forecasting (*Healy et al.*, 2007; *Cucurull et al.*, 2008).

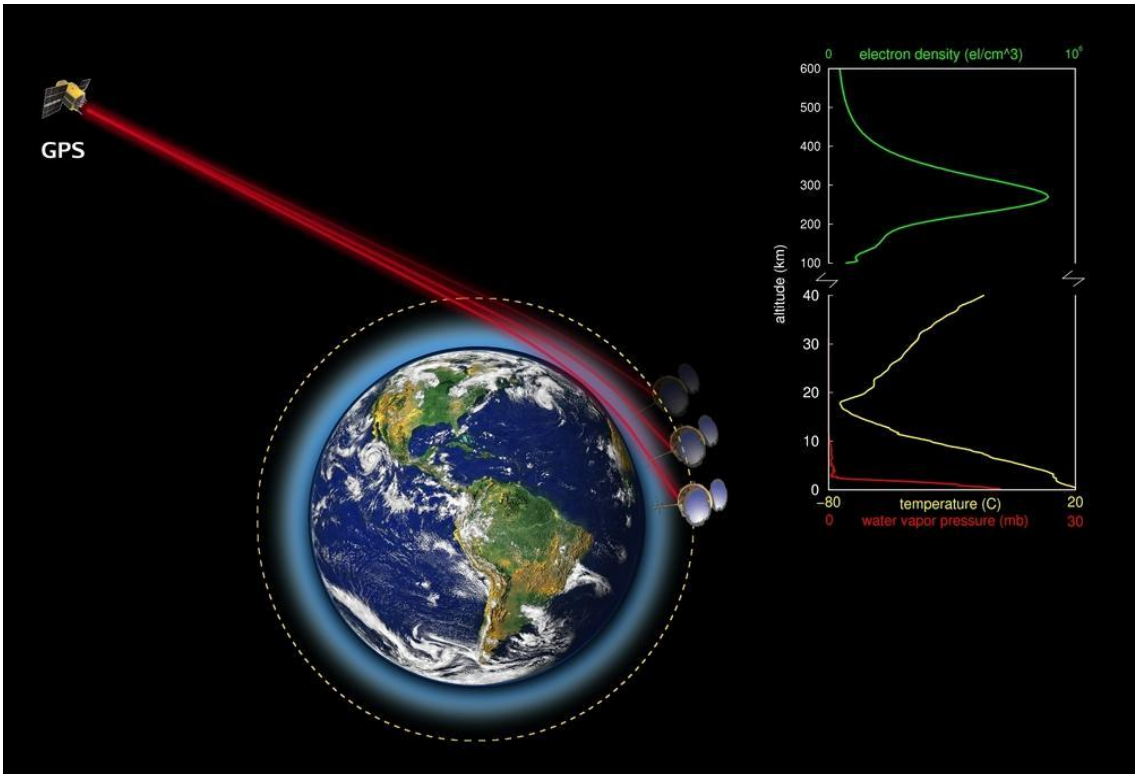

Figure 2 Illustration of the radio occultation scenario. Red lines depict the signal path from a GPS transmitting satellite to the receiver on orbiting LEO spacecraft. Over the course of several minutes, the signal path passes through different vertical regions of the atmosphere. The observed bending/delay of the signal can be analysed to estimate properties of the ionosphere and atmosphere.

Spire currently utilizes the radio occultation technique to provide both atmospheric profiles and ionospheric measurements on a daily basis. Each satellite in Spire's LEO constellation is equipped with a custom receiver that tracks GNSS signals at two different frequencies through multiple antennas. The main purpose of the high gain antenna, approximately aligned with the Spire satellite velocity direction, is to collect GNSS signals that pass through the atmosphere. Each occulted signal is tracked at 50 Hz sampling using a state-of-the-art, open-loop tracking technique (*Sokolovskiy et al.*, 2006), which employs an *a priori* model of the atmosphere to aid in the tracking of a GNSS signal. This technique is necessary to track the signal as it passes through the lowest portion of the atmosphere where signal dynamics are large and received signal amplitudes are degraded. A second upward-facing antenna is utilized to collect simultaneous, dual-frequency signals from multiple GNSS satellites at 1 Hz sampling for precise orbit determination (POD) purposes and derivation of ionospheric measurements. As explained in detail in later sections of this document, the determination of each Spire satellite position to an accuracy of several centimetres is crucial to obtaining accurate retrievals of atmospheric profiles during radio occultation measurements.

2.2.2 GNSS-RO Data Processing

The main purpose of this section is to explain how radio occultation data collected from each Spire satellite are processed to produce final atmosphere and ionosphere products. The atmospheric portion of the processing chain is comprised of three major steps (Figure 3): precise orbit determination, excess phase processing, and occultation inversion. All three segments of the atmospheric processing chain are briefly described within the subsections below.

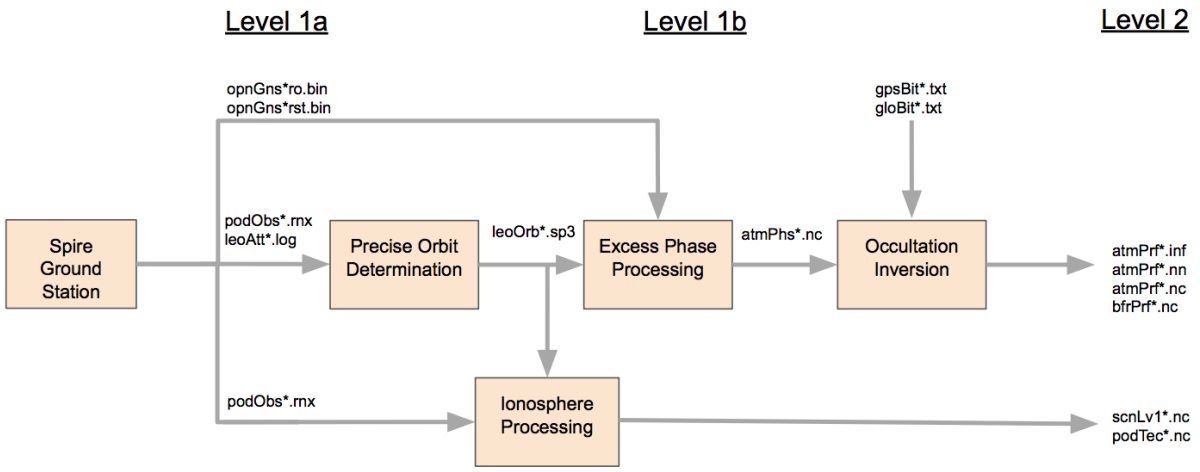

Figure 3 Overview of the atmospheric and ionospheric processing chain including raw, intermediate and final file formats assuming one Spire satellite. The block diagram begins with the raw data downlinked from the satellite to the ground and ends with the final atmosphere and ionosphere products.

Precise Orbit Determination

The inversion of GNSS occultation signals into atmospheric profiles of refractivity and temperature requires the accurate estimate of the signal bending angle as it passes through the atmosphere. One component necessary for the accurate estimation of signal bending angle is the precise position and velocity of both the GNSS satellite transmitter (~20,000 km above the Earth) and the Spire satellite receiver in a LEO orbit (~500 km above the Earth) during an occultation event. Due to the wide variety of applications using GNSS signals, the positions and velocities of each GNSS satellite are available through external sources and known to within several centimetres. This leaves the challenging task of estimating the position and velocity of the Spire satellite receiver to an accuracy of several centimetres and sub-mm/s, respectively.

To estimate each Spire satellite orbit, the Spire processing system employs a precise orbit determination software, RTOrb. The main inputs to the software are the orbital positions/velocities of each GNSS satellite and the pseudo-range and carrier phase measurements collected by the Spire receiver. The software computes the Spire satellite orbit position/velocity estimates at each time step by blending the input observations together with a complex orbit model through Kalman filtering. The orbit model accounts for both gravitational and non-gravitational forces, such as atmospheric drag and solar radiation pressure, which act on the Spire satellite as it orbits the Earth. Long (at least 50 minutes), continuous, dual-frequency observations of multiple GNSS satellites (at least 4 simultaneous) are required to achieve orbit estimates of less than 10 centimetres.

Once orbit positions are determined, Spire's processing chain includes excess phase processing to calculate the phase delay induced by atmospheric refraction. This excess phase, computed using an a priori atmospheric model, is then used to derive bending angle profiles, which serve as the input for further atmospheric property retrievals.

Excess Phase Processing

The other major component needed to estimate the atmospheric bending angle required for radio occultation inversion is the estimation of the relative signal phase delay induced by the Earth's atmosphere, which shall be referred to as "excess phase". The equation below shows how the excess phase in unit distance at each time step during the occultation event can be estimated given carrier phase observation (ρ), the straight-line distance between the GNSS and Spire satellite (R), and the receiver clock error multiplied by the speed of light ($c \cdot [\Delta clock]$).

$$\Delta\text{phase} = \rho - R - c \cdot \Delta_{clock}$$

Due to the open loop tracking mode of the receiver, the carrier phase observation (ignoring the ambiguity term) is actually a combination of two quantities: the *a priori*

phase model and residual phase measurements based on the difference between the modelled phase and the true signal phase. The straight-line distance, R, can be computed given the GNSS satellite transmitter and Spire satellite receiver orbit positions produced from the precise orbit determination. The receiver clock error imparts an error in the carrier phase observation (ρ) and consequently must be estimated and removed to compute a precise excess phase measurement. This task can be done by using simultaneous phase observations from a non-occulting GNSS satellite as a reference. It should be noted that the equation above is a simplification of the equation used in the processing software. The actual excess phase processing takes into account other minor corrections, such as the transmitter clock error, relativity terms, and transmitter and receiver phase offsets, in order to estimate the excess phase to within several centimetres.

Radio Occultation Inversion

The process of inverting the computed excess phase delay and orbit positions to profiles of atmospheric refractivity and temperature is briefly summarized here. Further details on the inversion techniques can be found in the references provided at the end of the document.

The excess phase delay is first pre-processed to remove half cycle and full cycle jumps. Half cycle jumps are mainly observed in the L1 excess phase delay due to 50 Hz navigation bit modulation of the GNSS signal. The effects of the navigation bits are removed from the excess phase delay by obtaining the GNSS navigation bits from an external provider. Full cycle phase jumps are caused by the residual phase wrapping inherent in the open loop tracking mode, which are removed after eliminating the navigation bit modulation effects.

After the excess phase delay is reconstructed, a time derivative of the excess phase is computed to obtain the Doppler frequency. Bending angle profiles as a function of impact parameter (see Figure 4 for illustration) can be obtained by relating the estimated Doppler frequencies to the occultation geometry consisting of the transmitter and receiver positions and velocities. This is commonly referred to as the geometric optical method. However, the geometric optical method breaks down when the signal passes through the lowest portion of the atmosphere due to multipath propagation and diffraction. In this region, a wave optical processing method must be employed, which takes into account the signal amplitude, excess Doppler frequency, and multiple ray path geometry to derive the bending angle profile. Further details on this method can be found in *Gorbunov and Lauritsen*, 2004 and *Gorbunov et al.*, 2011.

Once the bending angle profiles for both frequencies are obtained, a statistical optimization is applied to remove the effects of the ionosphere. Refractivity profiles can be retrieved from the bending angle profile by using an Abel transform (*Rocken et al.*, 1997). Finally, temperature profiles are obtained from refractivity profiles using the relation shown in Figure 4, along with *a priori* atmospheric information given from a model.

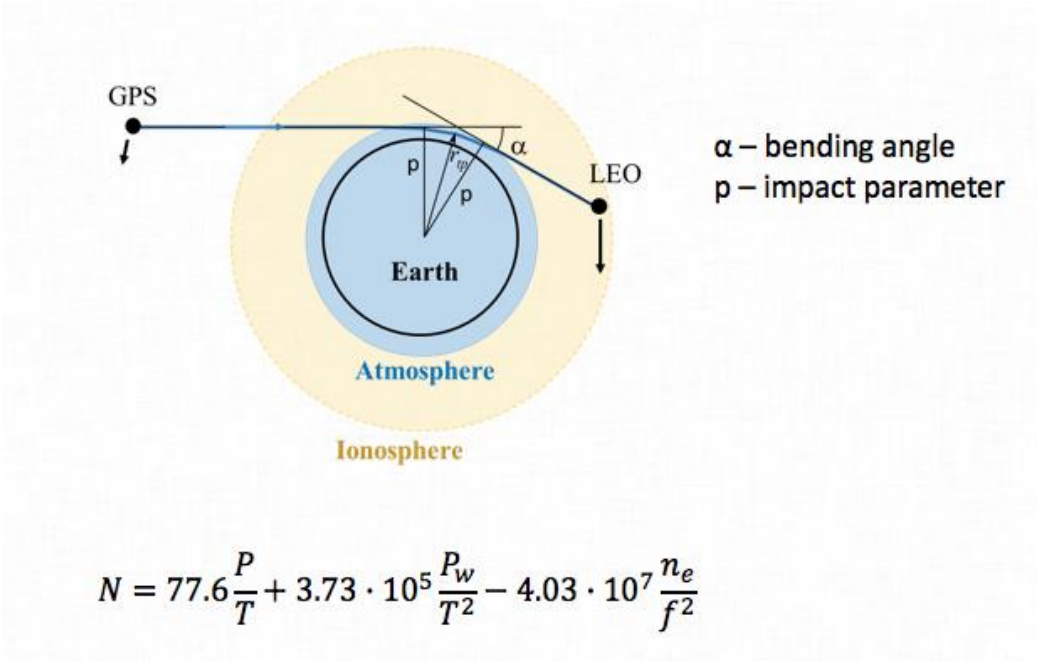

Figure 4 Occultation diagram illustrating the definition of bending angle and impact parameter. Bending angle profiles as a function of impact parameter allow for the derivation of atmospheric refractivity (N) profiles as a function of altitude. The relation between refractivity and temperature (T) as well as pressure (P), water vapor (P_w) and ionospheric electron density (n_e) is given in the equation contained in the figure.

An example of a temperature profile derived from radio occultation measurements collected by a Spire satellite is presented in Figure 5. The Spire-derived temperature profile is compared to the NOAA's Global Forecast System (GFS) weather model prediction, as well as temperature data derived from a radiosonde. From the plot, it can be observed that applying the radio occultation technique on Spire measurements can result in accurate temperature profiles from 40 km to the lowest few kilometres, which are crucial for weather forecasting.

Finally, it should be noted that although products of temperature and refractivity are produced by the radio occultation inversion process, the product that has the most value to weather forecasting models is bending angle. This is because the retrieval of refractivity and temperature profiles from bending angle by means of the Abel transform assumes a spherical symmetry of the atmosphere. The assumption decreases the value of these variables for assimilation by weather models because the atmosphere is not one-

dimensional and often has strong horizontal variability. Hence, bending angle is usually selected as the primary radio occultation data product for weather model assimilation.

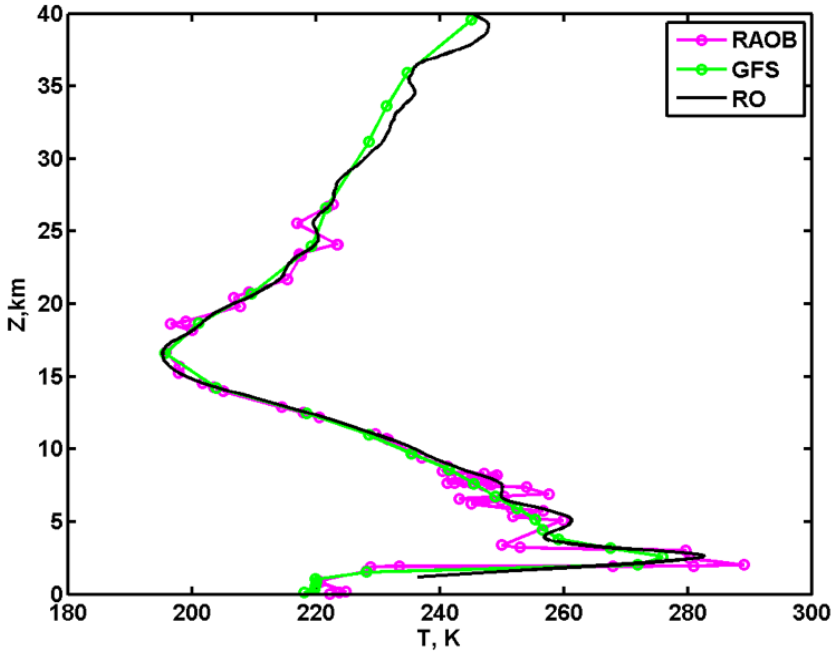

Figure 5 Example of a dry temperature profile derived from radio occultation data collected by a Spire satellite. The Spire observation is compared to a temperature profile predicted by the GFS weather model and temperature data obtained from a nearby radiosonde (RAOB).

Geolocation of RO profiles

RO profile can be seen as a sequence of rays. Each ray is characterized by impact parameter and bending angle and each ray has a point closest to the Earth ellipsoid WGS-84. This point has a latitude/longitude of its projection on the ellipsoid. One ray out of the whole sequence corresponds to the condition when a straight line (not the ray) between a transmitter and a receiver touches the ellipsoid. This touching point is called 'occultation point'. The occultation point is considered as a location of the whole RO profile. This location is used for statistical comparison with background profiles: either refractivity calculated at this point and time from interpolated atmospheric parameters, or bending angle calculated from that refractivity. During such a comparison we neglect horizontal variations of atmospheric parameters.

3D assimilation of RO measurement is done in a different way: it takes into account different ray trajectories at different impact parameters. The location, the azimuth, and the impact parameter are used to calculate model bending angles for each individual ray.

The best way to geolocate refractivity or dry temperature data is to use the location (i.e. latitude/longitude) of 'perigee point at occultation point' and assume that the profile is vertical. This assumption is more accurate for small boresight angles <= 30-40 degrees, and more questionable for larger angles. Refractivity and dry temperature given in netCDF and BUFR files are derived from RO data using Abel transform, which implies a spherically symmetric atmosphere in the area of sounding. It is impossible to reconstruct a 3D profile from RO data because each bending angle is accumulated over a ray trajectory in the atmosphere. A sequence of such integrals cannot be inverted into a profile in general 3D case, but it can be used as atmospheric soundings in data assimilation to numerical weather models.

2.2.3 Spire RO Production Volume

Due to its quantity of satellites and advanced GNSS-RO receiver technology, Spire has been the world's largest single commercial or government source of RO profiles since 2019. As shown in Figure 6, the Spire constellation has demonstrated the capability of collecting well over 15,000 quality-controlled RO profiles per day over an extended, multi-year period (mid-2021 to mid-2023). Spire was able to achieve these unprecedented large numbers of RO without fully utilizing the capacity of its satellites. The in-orbit capability was significantly higher but scaled back to share the constellation resources with other payloads to meet the demands from other customer applications. Despite the utilization below capacity, the Spire constellation produced over 3 times the amount of RO data generated by the next largest source, COSMIC-2, during this period. Furthermore, the Spire constellation has collected more RO profiles over the past 5 years than the COSMIC-1 (2008-2020) and COSMIC-2 (2019-current) constellations have during their orbital lifetime thus far.

Recommendations for RO are collated independently by the International Radio Occultation Working Group (IROWG) part of the Coordination Group for Meteorological Satellites (CGMS). One of the main recommendations since 2017 (IROWG-6 Report) has been "targeting at least 20,000 occultations/day providing good spatial and local time coverage" for the operational and research communities of NWP, Climate and Space Weather. The Spire constellation has almost single-handedly fulfilled the requirement for quantity by collecting over 15,000 profiles per day between late-2021 to mid-2023.

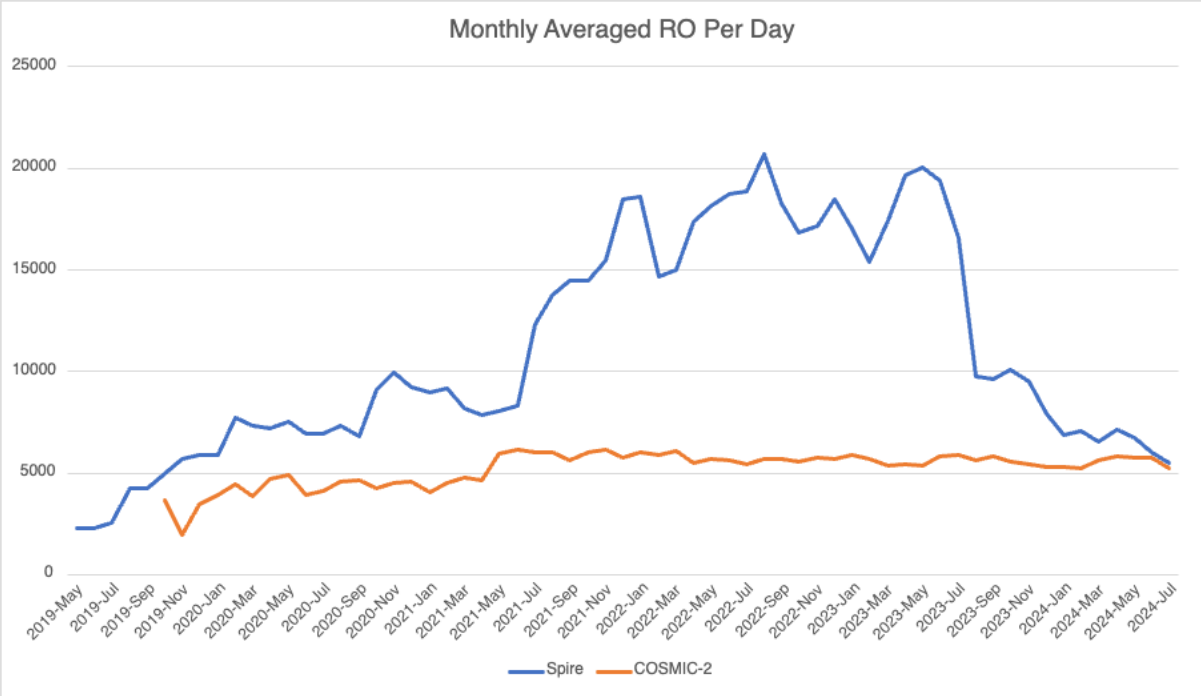

Figure 6 Spire and COSMIC-2 daily volume of quality-controlled RO profiles (monthly-averaged) between May 2019 and July 2024. COSMIC-2 counts obtained from https://gpsmet.umd.edu/gnssro/index.php

Satellites in Spire's constellation are also situated in a diverse set of orbital planes in low-earth-orbit, ranging from polar sun-synchronous orbits to mid and low inclination orbits. As a result, global coverage from Spire's RO observations is easily achieved over the span of 24 hours. Satellites situated in multiple orbital planes also allows Spire to collect RO observations over a large range of local hours, as recommended by the IROWG community (Figure 7). In the future, Spire plans to launch satellites into additional local time planes to provide more uniform spatial coverage over shorter timespans to maximize the impact on NWP and climate applications.

2.2.4 Spire RO Profile Quality

Formal data evaluations through government pilot programs and peer-reviewed research studies have shown that Spire RO data quality exceeds the requirements for NWP applications. Spire was one of two vendors that participated in NOAA's Commercial Weather Data Pilot Round 2 program (2018-2019) where it delivered at least 500 RO profiles per day over a two-month period. NOAA evaluated Spire's RO data quality and concluded that the data were comparable to other government platforms (Commercial Weather Data Pilot Round 2 Summary, 2020). Similarly, Spire RO data were assessed by EUMETSAT and the Wegener Centre in an ESA-funded study in 2020 (Quality Assessment of Commercial GNSS-RO Data, 2020). EUMETSAT also found that Spire GNSS-RO data in

the troposphere and stratosphere are comparable in quality to other operational missions and recommended the data for comprehensive data assimilation studies.

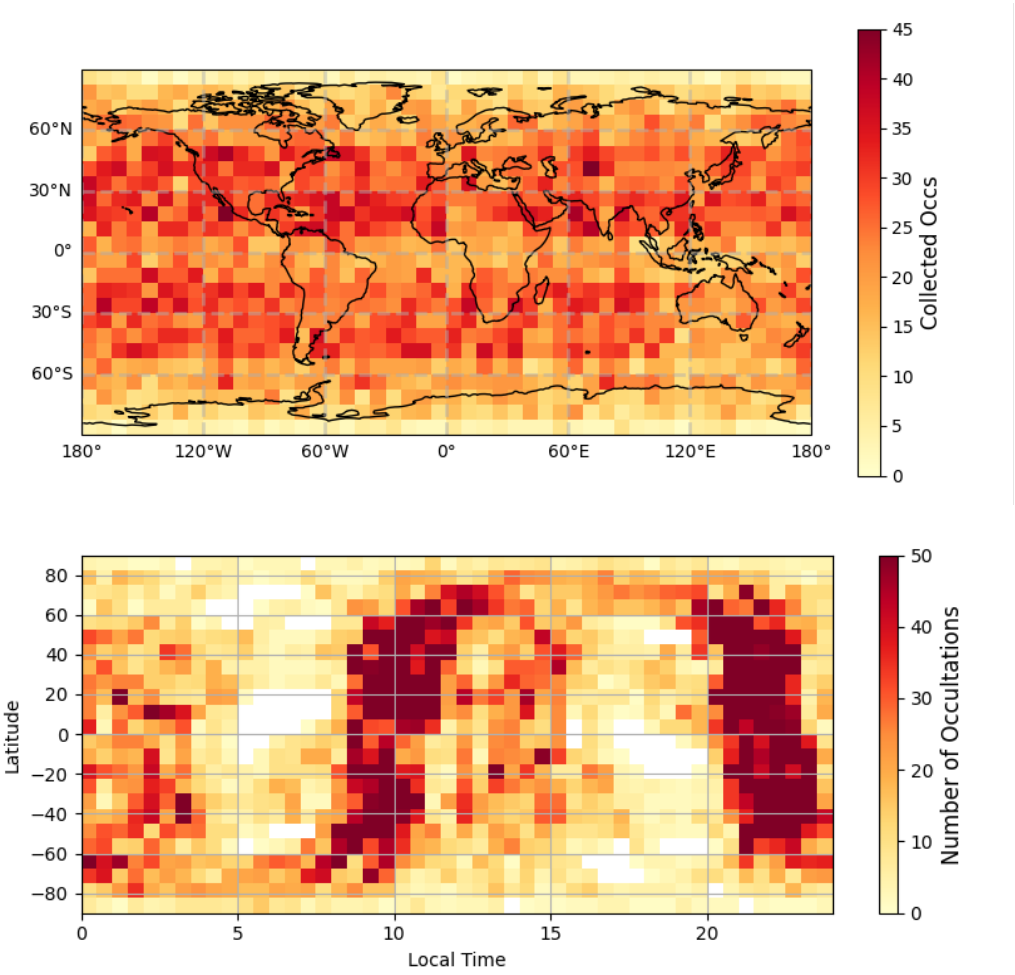

Figure 7 Number of RO profiles collected by the Spire constellation over 24 hours (September 1st, 2022). Top panel shows the number of RO profiles for each 7.5° x 7.5° latitude-longitude grid box and bottom panel displays the count for each 7.5° x 30-minute latitude-local time grid box.

However, the Spire constellation and its RO capabilities have rapidly progressed since the initial data evaluations and more recent peer-reviewed studies have been conducted. Most of these studies have concluded that Spire's RO data are comparable to COSMIC-2, which is considered NOAA's current backbone mission (Ho et al., 2022). By comparing RO bending angle profiles derived from the Spire and COSMIC-2 constellations using the same data processing system, Ho et al. 2023 concluded that "the precision of Spire STRATOS receivers is of the same quality as those of the COSMIC-2 TriG Receiver System". Spire and COSMIC-2 RO datasets have also displayed similar statistics on minimum penetration depth, one of the important weather parameters in the lower troposphere

(Jing et al, 2023; Ho et al, 2023; Weiss, 2022). One particular study even found Spire penetration depth exceeding COSMIC-2 in some regions (Qiu et al., 2023).

The conclusions from the aforementioned data evaluations and studies contradict previous assumptions that large satellites with high receiver signal-to-noise ratio (SNR) produce higher-quality RO retrievals than receivers with lower SNR values. The average reported COSMIC-2 SNR is approximately 4 times greater in amplitude than the average Spire value, which is to be expected due to COSMIC-2's larger antennas and satellite platform. Even after accounting for calibration differences that result in an overestimation of COSMIC-2 SNR values relative to Spire's (Gorbunov et al., 2022), conventional thought would incorrectly assume that COSMIC-2 RO data possess superior signal penetration depth and quality statistics in the lower troposphere where large signal variations and fading occur. The numerous independent studies over the past several years (see previous paragraph) have proven that this is not the case and receiver SNR is not a significant factor in determining RO quality.

2.3 GNSS-RO Data Assimilation

Atmospheric data from the Spire weather model has been leveraged in support of the FIRE-RES project. Global Navigation Satellite System - radio occultation (GNSS-RO) observations have been widely recognised by the Numerical Weather Prediction (NWP) community as one of the most impactful meteorological observations, along with conventional radiosonde, surface and satellite radiance (microwave and infrared) observations. Satellite missions such as Challenging Minisatellite Payload (CHAMP; Wickert et al. 2005) and FORMOSAT-3/Constellation Observing System for Meteorology, Ionosphere and Climate (FORMOSAT-3/COSMIC, Anthes et al. 2008) were pioneering GNSS-RO missions, that demonstrated great benefits for both weather forecasts and climate change studies. These benefits come from the global coverage of RO profiles which individually exhibit high accuracy, precision, and vertical resolution. In addition, GNSS-RO data provide measurements without bias thus helping with calibration of other data sources. It was concluded that the RO data were of similar quality as the radiosonde data, but with the advantage of global coverage across populated and unpopulated regions, such as oceans and the polar regions (e.g., Ho et al., 2020 and references therein). As a result, assimilation of GNSS-RO observations has become a standard practice in many weather forecasting centres.

Spire not only assimilates RO data collected by its own satellites, but also ingests data from COSMIC-2, MetOp/GRAS, TerraSAR-X, and Tandem-X satellites. Spire assimilates between 6,000 and 20,000 bending angle profiles on a typical day, which is higher than the amount assimilated from COSMIC-2 at centres like NOAA or ECMWF.

A typical bending angle profile consists of 200-400 measurements from about 2 km up to the upper stratosphere. In the lower troposphere, particularly below 5 km, the signal-to-noise ratio is lower, leading to higher uncertainty in the RO data.

2.3.1 Data Pre-Processing

Before assimilation, the bending angle measurements need to be converted into geophysical parameters (e.g., temperature and pressure) using established retrieval algorithms, such as the 1D NCEP Bending Angle Model (NBAM) as outlined by Cucurull et al. (2008). This conversion is essential for integrating RO data into Spire's data assimilation system.

Rigorous quality control measures are implemented to ensure that only reliable and accurate data are assimilated. This includes checks for gross errors, consistency with other observational data and the physical plausibility of the derived profiles.

A key enhancement in Spire's version of the NBAM algorithm is its ability to account for vertical error correlations in RO profiles. The strength of these correlations depends on the processing algorithm used to convert RO excess phases into bending angle profiles. Spire's algorithm achieves high vertical resolution (200 m) from altitudes below 2 km up to 70 km, resulting in stronger vertical error correlations compared to algorithms used by other meteorological centres. Analysis shows that Spire RO exhibits stronger error correlations below 20 km and stronger anti-correlations in the upper stratosphere, calculated using the Desroziers' method (Desroziers et al., 2005).

2.3.2 Data Assimilation Technique

Once processed and validated, the ingestion of RO data into the Spire data assimilation system is achieved using a hybrid 4DEnVar (Four-Dimensional Ensemble Variational Data Assimilation) technique, an advanced data assimilation technique used in numerical weather prediction (e.g. Kleist and Ide, 2015). 4DEnVar combines aspects of both ensemble-based and variational methods to improve the accuracy of atmospheric models.

Variational Data Assimilation

Variational methods, such as 4DVar (Four-Dimensional Variational Assimilation), solve an optimization problem to find the model state that best fits the observations over a time window. They rely on a static background error covariance matrix, which represents uncertainties in the initial model state. While effective, traditional 4DVar approaches are limited by their assumption of static error structures, which can oversimplify the representation of forecast uncertainty.

Ensemble-Based Data Assimilation

Ensemble methods, such as Ensemble Kalman Filters (EnKF), use a collection of model forecasts (an ensemble) to dynamically estimate error covariances. These methods are highly effective in capturing atmospheric flow-dependent uncertainties, providing a more accurate representation of the evolving state of the atmosphere.

Hybrid Approach in 4DEnVar

The hybrid 4DEnVar technique merges the *variational* and the *ensemble-based* approaches by using ensemble-generated background error covariances to augment the static covariances in variational methods. This hybridisation allows the assimilation system to dynamically adjust to changes in the atmosphere while maintaining the computational efficiency of variational approaches. The resulting method retains the four-dimensional aspect of variational methods, where observational data is assimilated across a time window, but it also benefits from the dynamic, flow-dependent error estimates provided by the ensemble. This is particularly valuable in scenarios with high observation density, such as the ingestion of Spire's RO data.

2.4 Impact on GNSS-RO on Forecast Systems

The benefits of Spire RO data to NWP have been evaluated internally at Spire and externally. The external studies were particularly informative and valuable to Spire, since those were performed using different forecast models and data assimilation systems, thus providing complementary analysis on the impact of Spire RO data.

For example, Bowler (2020) focused on the impact of Spire RO data on the UK Met Office global NWP system, which employed a hybrid four-dimensional variational (4D-Var) data assimilation method. Bowler (2020) examined the impact of Spire RO data by performing Observing System Experiments (OSEs). They performed three main experiments over the period of three months (8 September 2019 - 8 December 2019): (1) Removing all GNSS-RO data from the system, then (2) including Spire RO data to the system, and finally (3) replacing Spire RO data by the MetOP-C data. The study concluded the following: “Assimilating observations from Spire in addition to the current operational network brings substantial benefits to forecast performance. These benefits are seen for almost all forecast variables and lead times. However, the reductions in the Root Mean Square Difference (RMSD) between the forecast and the verifying analysis are much smaller than the detriments seen from removing all operational GNSS-RO observations, despite this being a smaller number of observations. Removing data from Metop-C and replacing it with an equivalent number of observations from Spire leaves the system approximately unchanged. Therefore, we conclude that the two data sources are of similar quality.”

The Bowler (2020) study also quantified the overall impact of all assimilated GNSS-RO data on reducing the forecast Root Mean Square Error (RMSE) with respect to the verifying ECMWF analysis, as well as verifying observations, and concluded that there is a logarithmic dependence between the number of occultations (Noccs) per day and the percentage or RMSE reduction (Figure 8). The greatest error reduction (1.21 %) was obtained when the maximum number of RO profiles (7,000 RO profiles) were assimilated per day. The forecasts were initialized twice per day (at 00z and 12z) and verified against the ECMWF analyses (black line).

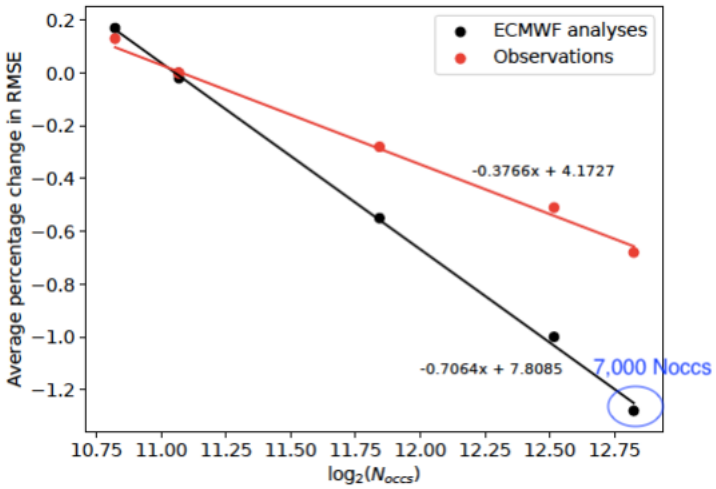

Figure 8 Average forecast RMSE reduction (%) as a function of the logarithm of the number of occultations (Noccs) per day. Note that, for the maximum number of GNSS-RO profiles assimilated (7,000 Noccs per day), the forecast error reduction, measured with respect to the European Centre for Medium-Range Weather Forecasts (ECMWF) analysis (black line), was estimated to be 1.21 %. Also note that the forecast error reductions with respect to the observations follow similar logarithmic dependence (red line), but are typically smaller, however the observations are sampling the globe in a less uniform way than the ECMWF analyses (Figure taken from Bowler 2020)

Note that assimilation of 7,000 RO profiles is far from the expected saturation of RO benefits (e.g., Harnisch et al. 2013). Harnisch et al. (2013) examined the potential impact of synthetic RO profiles as a function of the number of those profiles. They determined that, although the magnitude of positive impact gradually decreases as the number of RO profiles increases, there is no saturation of the benefit up to at least 128,000 RO profiles per day.

An alternative way to measure the impact of assimilated observations on the forecast improvement, and less computationally expensive than OSEs, is evaluating a metric called Forecast Sensitivity to Observation Impact (FSOI, Langland and Baker, 2004, Cardinali 2009). A study performed at the ECMWF (Healy 2020) belongs in the category of the FSOI-type studies. They also found significant benefits of Spire RO data, as well as COSMIC-2 data, especially during the period in 2020 when the amount of assimilated aircraft data was significantly reduced due to COVID flights restrictions. Results from Healy (2020) are shown in Figure 9. It can be seen that there is an increase in FSOI for GNSS-RO data (denoted GPSRO, orange line in the figure) at the time when COSMIC-2 was introduced, then additional increase when Spire RO was included and finally a decrease when Spire RO was removed. It is also evident that GPSRO data is among the five most impactful observations, together with microwave water vapor (MWWV) radiance, microwave

temperature (MWT) radiance, infrared temperature (IRT) radiance and infrared water vapor (IRWV) radiance data.

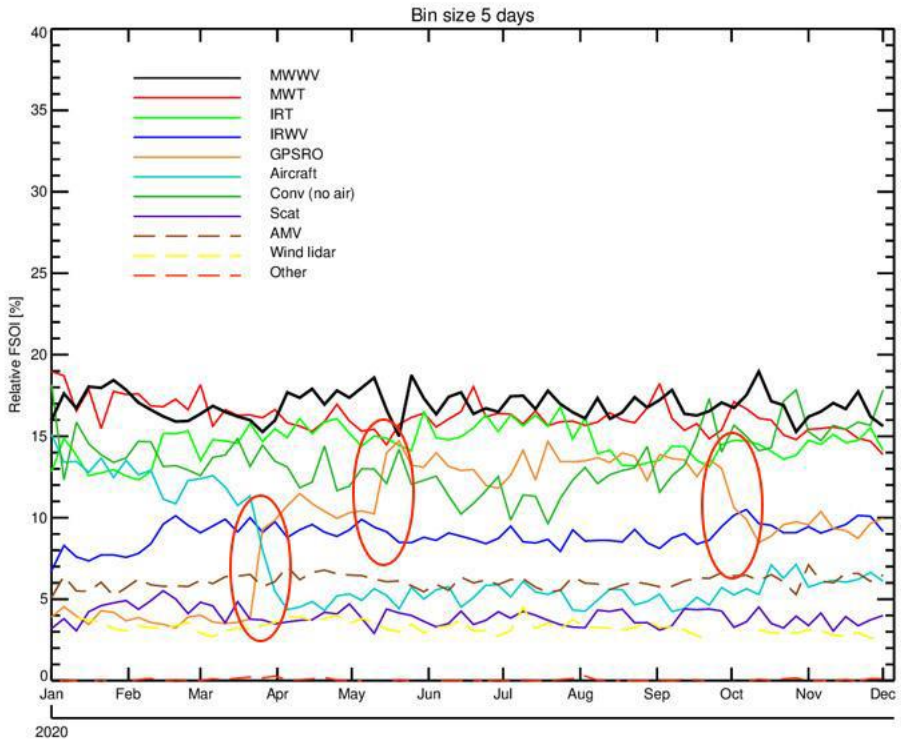

Figure 9 The operational Forecast Sensitivity to Observation Impact (FSOI, Cardinali 2009) timeseries, calculated as relative FSOI % for 24 h forecasts. The GNSS-RO (called GPSRO in figure) contribution is the orange line. COSMIC-2 was assimilated on 25 March 2020 and Spire on 13 May 2020. Spire RO was assimilated until 30 September 2020. Note the red circles indicating an increase in GPSRO FSOI (orange line) at the time when COSMIC-2 was introduced, then additional increase when Spire RO was included and finally a decrease when Spire RO was removed (Figure taken from Healy 2020)

2.5 Spire Weather Model Data Deliverables

The data assimilation system, described in section 2.3.2 Data Assimilation Technique, is used to define the initial conditions for the Spire global forecast model. Spire leverages the community-based Unified Forecast System (UFS) with Finite-Volume Cubed-Sphere (FV3) dynamical core (Harris and Lin 2013). Version 15 of this model (UFS-FV3.v15) is implemented into Spire operations, which is called 'SOFD' (an acronym for Spire Operational Forecast - Deterministic).

The SOFD model is run at 13 km horizontal grid-spacing and has 64 layers in vertical with model top at ~ 54 km. The data is outputted on a cylindrical 0.125° lat/lon grid. The SOFD model runs four times per day. The model issuances at 00UTC and 12UTC are long runs and produce forecasts up to 15 days into the future. The model issuances at 06UTC and 18UTC are shorter runs and produce forecasts out to 24 hours into the future.

The SOFD forecast data is available through the Spire Weather API through either point requests or file request. A point request returns forecast data (in JSON format) for a geographical location specified by a latitude-longitude combination. The file request returns gridded data (in GRIB format) for predefined regions.

In the scope of this project, output data of Spire's SOFD model is accessible as visualisation layers through the Integrative Software System (ISS). More information on the ISS and Spire's weather data can be found in the deliverable *D5.2 IA5.1 brief: Integrative umbrella system for EWE decision-making*.

3.PART 2 – VEGETATION DATA COLLECTION

The methodologies developed in this section correspond to the work carried out in Innovative Action (IA) 5.3 over Catalonia's Living Lab (CAT), with the main objective of developing new methodologies based on remote sensing datasets to monitor the evolution of key forestland metrics and phenological parameters and to integrate the generated data in an web-based platform in order to facilitate their accessibility and distribution.

This IA 5.3 stems from the Subtask 5.2.1 *Advanced vegetation characterization based on Earth Observation (EO) data fusion and Artificial Intelligence (AI) over forestland ecosystems*. Data fusion of optical EO, multi and hyperspectral datasets and LIDAR data under AI approaches to map forestland fuel conditions, derived water content parameters, changes and tendencies, monitor post-fire scenarios regarding vegetation recovery coupling EO data with ecological and socioeconomic factors on agile decision making geoservice tools.

3.1 Overview

Within the framework of advanced vegetation characterization based on Earth observation data, the first methodologies are primarily focused on estimating the CO_2 emissions resulting from wildfires. To achieve this, wildfire severity is first assessed using the differenced Normalized Burn Ratio (dNBR) (Key & Benson, 2006), a widely recognized index for detecting and measuring the impact of fire on vegetation. The dNBR allows for a clear evaluation of burn severity, which is essential for understanding the scale of biomass loss and subsequent carbon emissions (Wiedinmyer et al., 2006). Following this, an estimation of biomass loss in tons is carried out, taking into account not only the volume but also the specific types of forest cover affected. This distinction is crucial because different forest types have varying biomass densities and carbon storage capacities, which directly influence the amount of CO_2 released into the atmosphere.

In parallel, the methodologies also include an in-depth analysis of multi-temporal remote sensing data. Specifically, a time series analysis of Sentinel-2 imagery over the 2015-2024 period is conducted, focusing on the extraction of various vegetation indices. These indices, such as NDVI (Normalized Difference Vegetation Index) and VGI (Vegetation Growth Index), provide critical insights into vegetation health, phenological changes and post-fire recovery dynamics. The long-term monitoring enabled by this time series approach is invaluable for tracking gradual changes in forestland and identifying patterns of recovery or degradation over time.

Moreover, these time series datasets, derived from Sentinel-2 images, are intended to be further exploited using advanced artificial intelligence (AI) models. By applying AI and machine learning techniques, the aim is to uncover hidden trends and predict future forestland dynamics with greater accuracy. The combination of remote sensing data and

AI allows for the development of predictive models that can assess not only past and present vegetation conditions but also forecast future changes, thus offering a powerful tool for forest management, wildfire risk assessment and climate change mitigation.

In summary, the methodologies developed encompass a comprehensive approach to wildfire impact assessment and long-term forest monitoring. By integrating remote sensing data, biomass estimation, and AI-driven analysis, the project aims to enhance our understanding of forest ecosystem dynamics, improve our ability to measure and mitigate CO_2 emissions from wildfires, as well as contribute to more effective forest management strategies in the face of climate change.

The methodologies described were developed using various wildfires in the Catalonia Living Lab as tests. The wildfires selected had to be after June 2015 (Sentinel-2 mission service start) with a variety of burnt areas size, bioclimate regions and land cover. Figure 10 shows the localization of the selected wildfires.

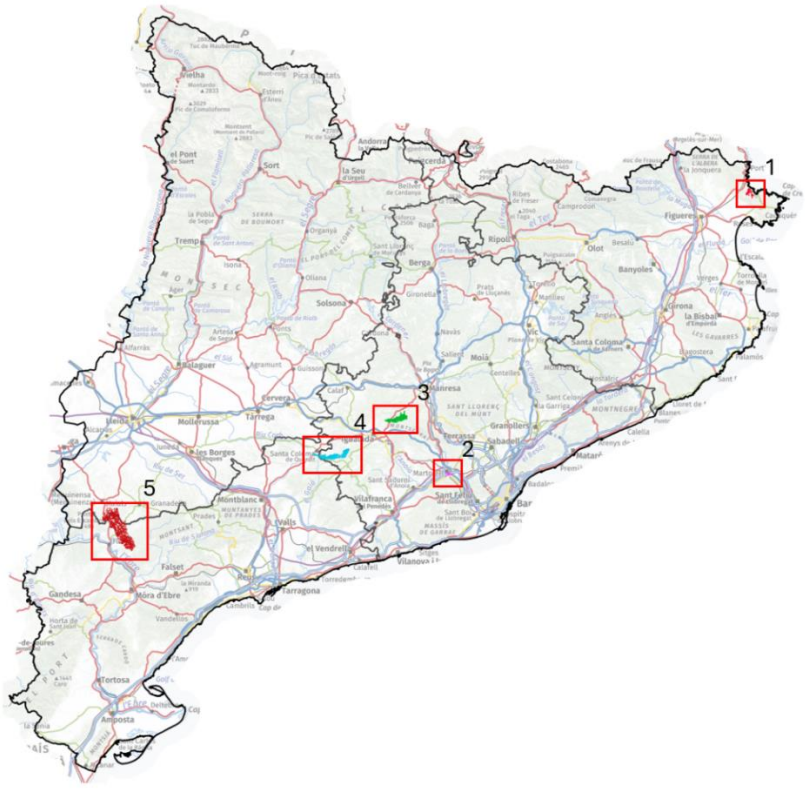

Figure 10 Map of Catalonia LL with the localization of the studied wildfires

1. Llançà fire (16-07-2021) burned approximately 415 hectares in the Cap de Creus Natural Park, a Mediterranean Northern coastal region under strong winds and dry conditions. The affected area was mostly covered with maquis shrubland and dispersed small pines.

2. Martorell fire (13-07-2021) is considered a smaller fire compared to the others, with an estimated range of 200 hectares burned, but it is important to highlight its proximity to big urban areas. It was located in the Baix Llobregat area, sharing the typical Mediterranean climate with pine forests and shrub zones.

3. Òdena fire (26-07-2015) approximately had 1,300 hectares burnt. It is in the central inland part of Catalonia, where the Mediterranean climate has some continental characteristics with wider temperature variations and less coastal influence. The main vegetation affected was mostly dense pine forests.

4. Santa Coloma de Queralt fire (24-07-2021) had over 1,700 hectares burnt. Also located in the central inland of Catalonia, in a predominantly rural environment with mixed agricultural and forested areas typical of the Mediterranean climate, where dry summers make the region prone to wildfires.

5. La Torre de l'Espanyol fire (26-06-2019) burned around 6,000 hectares being one of the biggest wildfires in Catalonia in recent years. Located in the Ribera d'Ebre region, this area is known for its Mediterranean climate with hot and dry summers, which contributed to the fire's rapid spread.

3.2 Severity and Biomass Consumption Estimation

3.2.1 Severity

The severity of a burned area refers to the accumulated effect on the ecological communities that make up the landscape after the fire. This includes both physical and chemical changes in the soil. The scope covers all degrees of impact, culminating in the most extreme case, where essentially all organisms are eliminated, and the community must regenerate from scratch. Severity makes sense as long as it is understood to refer to the conditions left behind after the fire.

Using remote sensing methods, the severity can be estimated with the Normalized Burn Ratio (NBR) index. The use of this index is justified by the fact that reflectivity in the Near Infrared (NIR) band responds positively to vegetation cover and wet areas, while the Short-Wave Infrared (SWIR) band responds to dry land and non-productive surfaces. The combination of these bands using the equations shown below will indicate where changes in vegetation cover have occurred and the magnitude of these changes.

The NBR is, therefore, a normalized index with a range from -1 to 1. When applied to different satellites, the bands used will be bands 4 and 7 for the TM and ETM+ sensors of Landsat 5 and Landsat 7, and bands 5 and 7 for Landsat 8 (OLI+TIRS), while for Sentinel 2, the bands used will be 8 and 12. This index provides the best contrast between healthy photosynthetic vegetation and burned vegetation.

$$NBR = (NIR - SWIR) / (NIR + SWIR)$$

The final index that we will use is a differential of the NBR (called delta NBR, dNBR), which is the difference between the NBR value from the image closest to the fire's start date (NBRpre) and the image available closest to the fire's end date (NBRpost). In the severity maps where the dNBR is applied, broad categories are shown in Table 2:

$$dNBR = NBRpre - NBRpost$$

Table 2 Severity level equivalences

Severity Level	dNBR value
Unburned	< 0.1
Low	0.1 - 0.27
Moderate	0.27 - 0.44
High	0.44 - 0.66
Very High	>= 0.66

In the Figure 11 can be appreciated the NBR maps before and after the wildfire of the 26th July 2015 in Òdena, and then, Figure 12 illustrates the results of the classified dNBR for the same wildfire. The dNBR is calculated using the 16 July 2015 image as the closest cloudless Sentinel-2 pre-fire image and the image of the 2 August 2015 as post-fire.

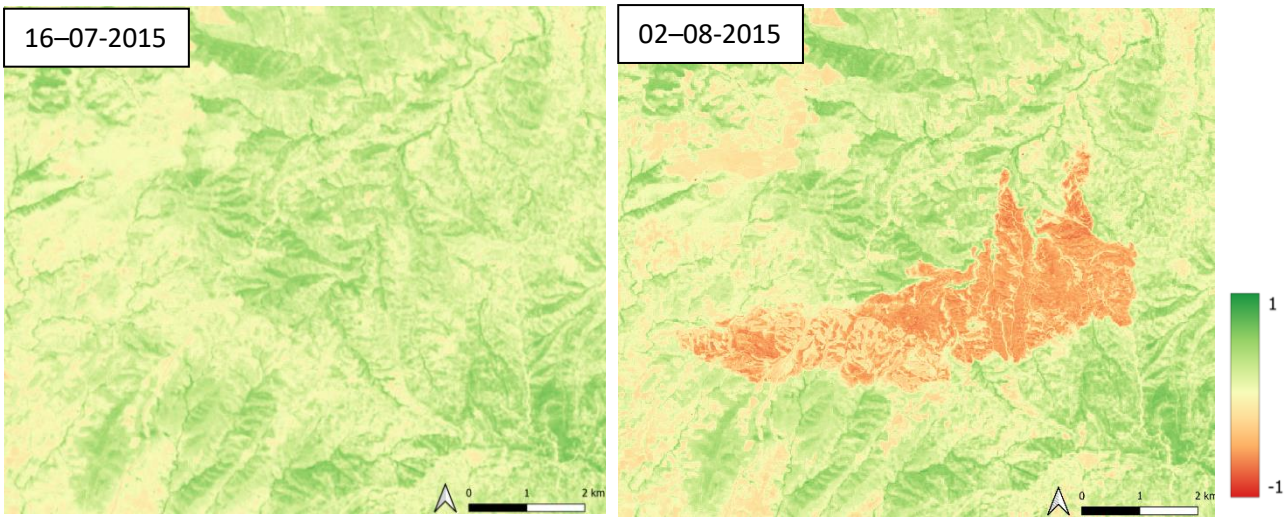

Figure 11 NBR Indexes before (left) and after (right) of the Òdena's wildfire

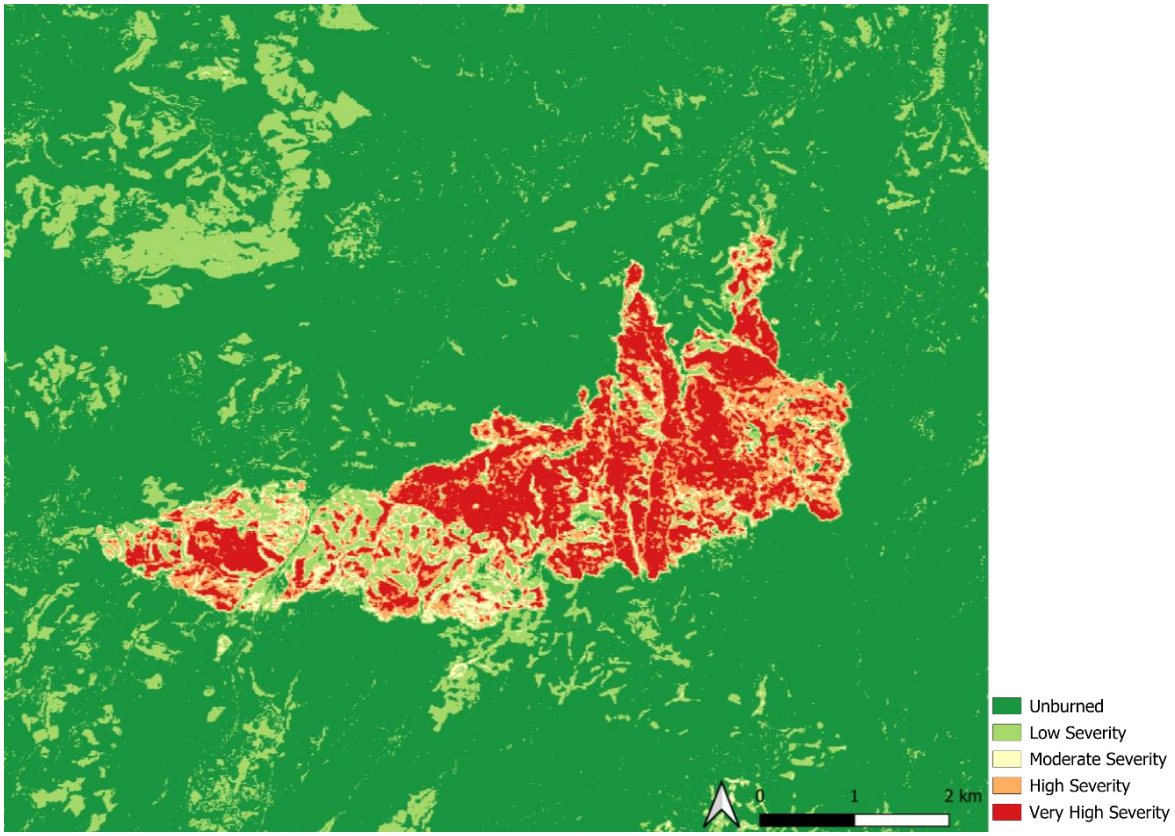

Figure 12 Classified dNBR of Òdena's wildfire, 2015

3.2.2 Biomass Consumption

Greater severity leads to greater biomass consumption and a larger loss of the forest system. Losses are estimated through the relationship established in previous studies between severity, explained by the dNBR index and the percentage of biomass consumed for each type of vegetation. Therefore, by knowing the severity and the pre-existing biomass, it is possible to estimate biomass losses (De Santis et al., 2010). The proposal by De Santis et al., 2010 is based on a study and subsequent publication where consumption factors for Mediterranean climate areas in a California forest were proposed. We consider these factors to be the most appropriate to apply to our latitudes, given the few published factors available.

By reclassifying severity into intensity (Table 2) according to the work of Key and Benson 2006, we can relate it to biomass consumption values based on severity levels and vegetation types (Table 3). By multiplying the pre-existing biomass by the factor attributed pixel by pixel and then summing all the pixels, we obtain the total biomass consumed in tons.

Table 3 Table of coefficients of Biomass Consumption per severity level and type

Severity Level	Consumed Biomass		
	Coniferous	Broad-leaved	Shrubs
Low	0,25	0,25	0,71
Moderate	0,47	0,4	0,84
High	0,56	0,48	0,89
Very High	0,65	0,56	0,95

To obtain the vegetation type, in the case of CAT Living Lab, there is a precise, detailed and updated land cover map (*Mapa de Cobertes del Sòl de Catalunya*) produced by the ICGC, which offers 12 distinct vegetation types, that need to be grouped in the 3 categories (Coniferous, Broad-leaved or Shrubs). Otherwise, products like the Corine Land Cover or the European Space Agency (ESA) World Cover can be exploited to obtain a vegetation classification.

3.3 CO_2 Emissions Estimation

Once the Coefficient of Consumed Biomass is assessed, the pre-existing biomass (in tons) must be determined to calculate emitted CO_2. For the case of Catalonia LL, the Forestry Biophysics Variables Map (ICGC, CREAF) is used to estimate biomass. As shown in Figure 13, the Biophysics Variables Map provides biomass density data with a 20 x 20 metres spatial resolution. To obtain the absolute mass per pixel, we multiply the density by the pixel area, expressed in hectares.

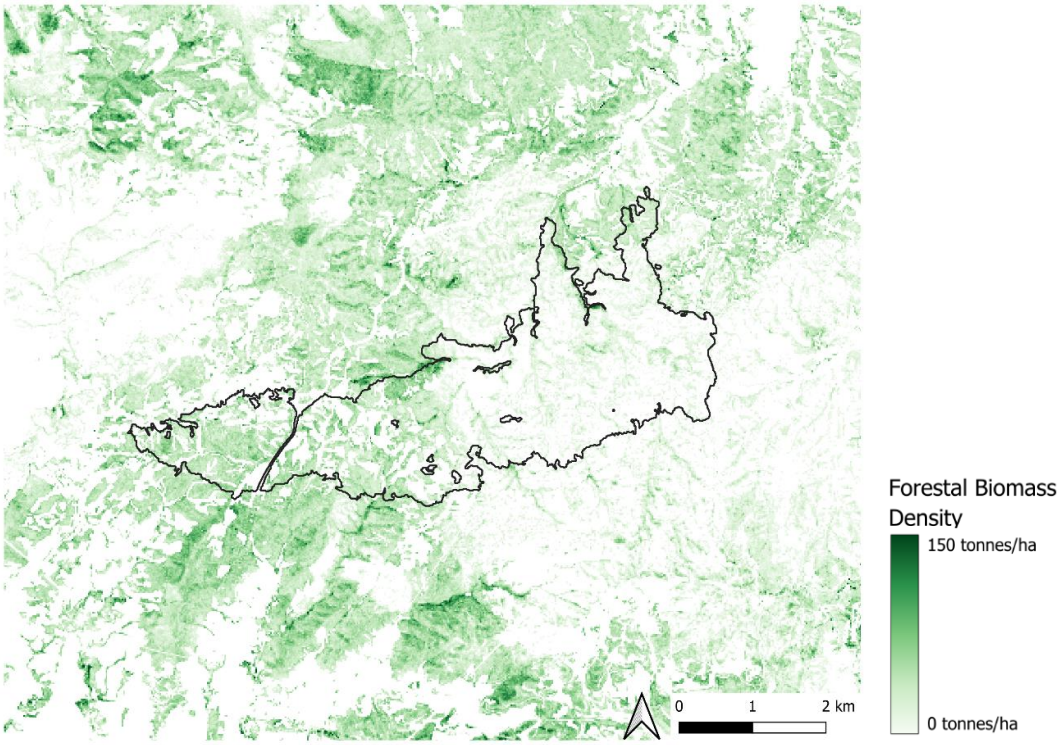

Figure 13 Forest biomass density of the Forestry Biophysics Variables Map (ICGC, CREAF) with Òdena's wildfire marked as a black line

As established in the work of Wiedinmyer et al. (2006), each type of gas released during the combustion of trees and shrubs has a specific Emission Factor (EF). For instance, burning 1 ton of wood, combined with oxygen, generates approximately 1.58 tons of CO_2. The EF is expressed as mass emitted per mass consumed, typically in kg/Mg.

To calculate the emitted CO_2, we can apply the formula described by Wiedinmyer et al. (2006) combining the pre-existing biomass, the consumed coefficient and the emission factor:

$$CO_2 \text{ Emissions} = B * CB * EF\ (CO_2)$$

Where:

B = Pre-existent Biomass (tons).

CB = Consumes Biomass (0 to 1 coefficient).

EF = Emission Factor (kg/Mg of gas per consumed ton).

Figure 14 presents the results from the formula, displayed on a map. Additionally, Table 4,

Table 5 and Table 6 summarize the biomass burned, by type (coniferous, broad-leaved and shrubs, respectively), and the CO_2 emitted. This analysis covers the five wildfires defined in Figure 10 and all information is accessible via Technosylva's ISS platform (https://iss.fire-res.com).

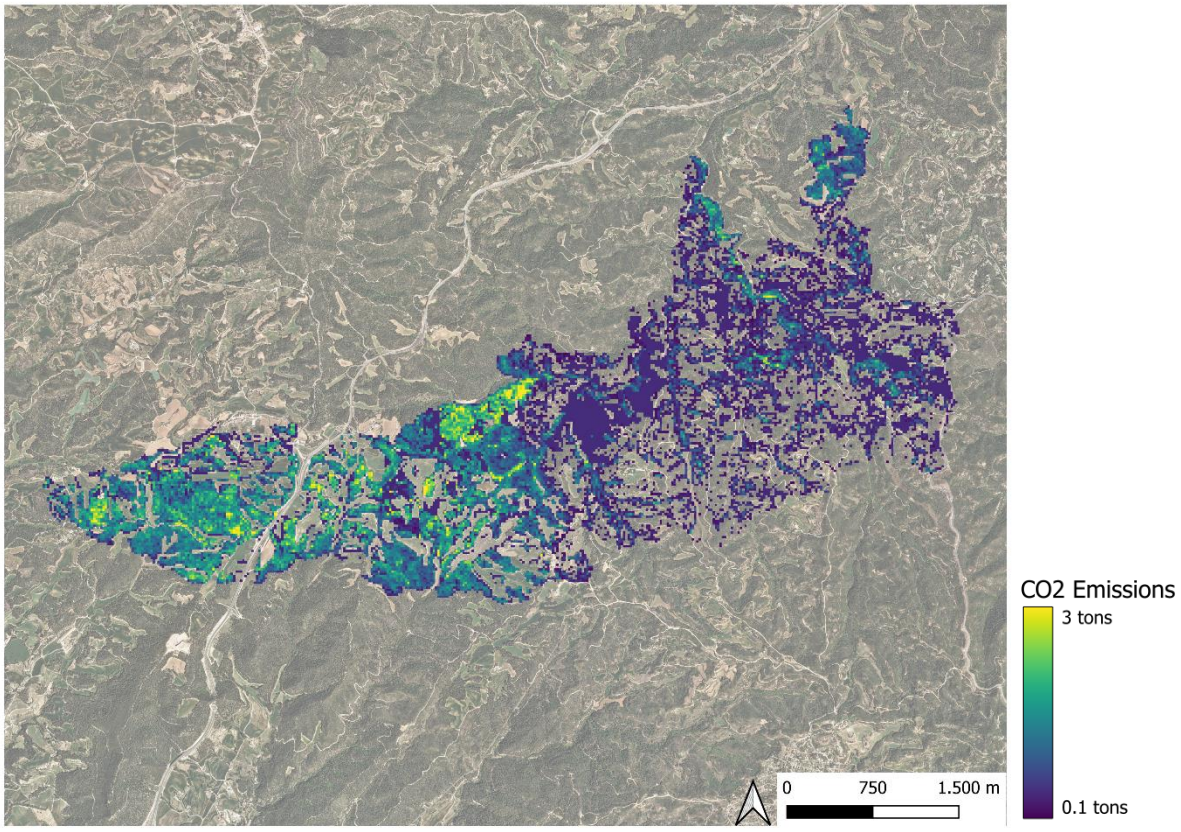

Figure 14 CO_2 emissions map for Òdena's wildfire. Background: 2015 Catalunya's flight orthophoto (ICGC)

Table 4 Summary table of coniferous type in Òdena's wildfire analysis.

Severity Level	Burned Surface (ha)	Burned Biomass (t)	CO_2 Emissions (t)
Low	28,80	247,78	341,20
Moderate	74,60	1203,59	1657,34
High	172,44	2973,77	4094,88
Very High	331,92	5913,65	8143,09
TOTAL	607,76	10338,79	14236,51

Table 5 Summary table of broad-leaved type in Òdena's wildfire analysis.

Severity Level	Burned Surface (ha)	Burned Biomass (t)	CO_2 Emissions (t)
Low	0,68	9,62	13,24
Moderate	0,68	12,05	16,59
High	1,24	30,88	42,52
Very High	4,84	119,96	165,19
TOTAL	7,44	172,50	237,54

Table 6 Summary table of shrubs type in Òdena's wildfire analysis

Severity Level	Burned Surface (ha)	Burned Biomass (t)	CO_2 Emissions (t)
Low	11,76	68,62	94,49
Moderate	28,92	196,50	270,57
High	55,04	402,31	553,98
Very High	36,60	279,54	384,92
TOTAL	132,32	946,96	1303,96

3.4 Indices Time-Series analysis and AI methodologies

In parallel to characterizing vegetation at the moment of the wildfire, a nearly decade-long analysis of Sentinel-2 images from 2015 to 2024 was conducted to explore the broader temporal dynamics of affected landscapes, mostly using representatives' vegetation indexes such as NDVI and VGI. This time-series approach aids in understanding how prior vegetation conditions, such as seasonal growth patterns or drought-induced stress, contribute to wildfire severity while also revealing recovery patterns after the event. By utilizing AI to process and interpret these indices, we can detect nuanced shifts in vegetation health and resilience, ultimately informing predictive models that assess future wildfire risk based on historical trends and current ecosystem vulnerabilities.

3.4.1 Indices Time-Series

By combining the revisit times of both Sentinel-2A (since 2015) and Sentinel-2B (since 2017) satellites, we achieve a temporal resolution of approximately 5 days, allowing for around 70 potential images per year for each study area. However, cloud cover limits usable data, requiring us to filter out images with significant cloud presence. For each of the five wildfire's study areas, we processed over 600 images but ultimately utilized between 200 and 250 cloud-free images, depending on cloud frequency and location. For instance, in the case of the Torre de l'Espanyol wildfire, we analysed a total of 217 cloudless Sentinel-2 images. This specific wildfire will serve as an example throughout our analysis to illustrate the methodologies applied and demonstrate possible outcomes.

As mentioned, in the analysis of the wildfire of Torre de l'Espanyol, 217 images were used. The following Table 7 shows its distribution for every year. Figure 15 and Figure 16 work as summaries showing one image per year (during summer) for NDVI and VGI indexes, respectively.

Table 7 Cloudless Sentinel-2 images per year used in the analysis. Starting at 23/06/2015 up to 28/06/2024

Year	2015*	2016	2017	2018	2019	2020	2021	2022	2023	2024*	TOTAL
N° S2 Images	3	13	33	28	30	24	24	21	28	13	217

*Incomplete years

The NDVI represents the vegetation vigour, providing insight into the overall health and density of plant cover, while the VGI represents the growth of the vegetation (A. Tardà, 2022), serving as an indicator of the rate of vegetation increase over time. This dual approach allows us to capture both the vitality of the vegetation and its growth dynamics, which are critical for understanding ecosystem responses before and after wildfire events.

In both time series, the impact of the June 2019 wildfire event is clearly visible, marked by a sharp drop in index values immediately following the event. At a deeper level, however, we can observe a gradual recovery within the affected zone, reflected by a yearly increase in the index values, indicating slow but steady regrowth. Meanwhile, the surrounding areas show a slight decline in these values, attributed to a prolonged three-year drought that has impacted vegetation health beyond the burned area. This contrast highlights the combined effects of wildfire recovery and drought stress on vegetation dynamics in the region.

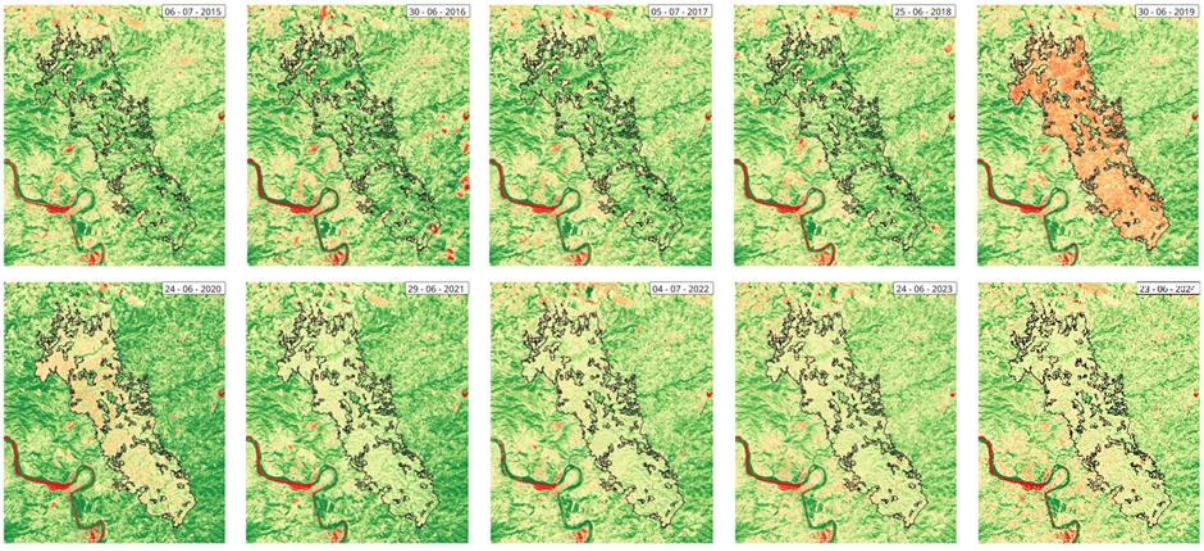

Figure 15 Evolution of NDVI. 1 image per year of Torre de l'Espanyol wildfire

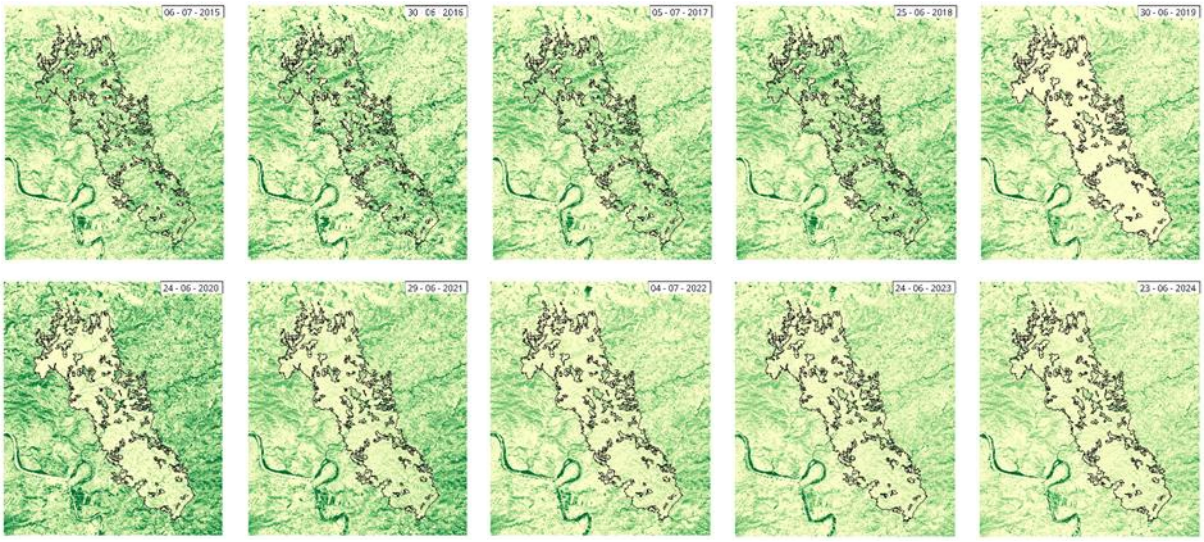

Figure 16 Evolution of VGI. 1 image per year of Torre de l'Espanyol wildfire

3.4.2 AI Model Development

The information that comes out of the multilevel analyses of the 10-year time series is the key to develop a model based solely on worldwide free access Sentinel-2 images and historic weather data. At this moment, the Multilayer Perceptron (MLP) deep learning model is being developed using the following weighted inputs:

- Burned area indexes time-series values.
- Control zones indexes time-series values.
- Trend difference between burned and control zones.
- Daily precipitation data.
- Daily temperature data.
- Daily humidity data.

To capture the unaltered dynamics of the forest ecosystem, we use two weighted control zones for comparison. As shown in Figure 17, the first control zone is a 1-kilometre buffer around the burned area, while the second is a 5-kilometre buffer around the first. Using two control zones instead of a single large one allows us to assign greater weight to vegetation closer to the burned area, as it is more ecologically similar. However, to mitigate the potential influence of outliers (which could skew results significantly in the immediate vicinity) the second larger buffer zone helps to balance the data. This approach provides a more accurate baseline for evaluating recovery trends and broader forest dynamics.

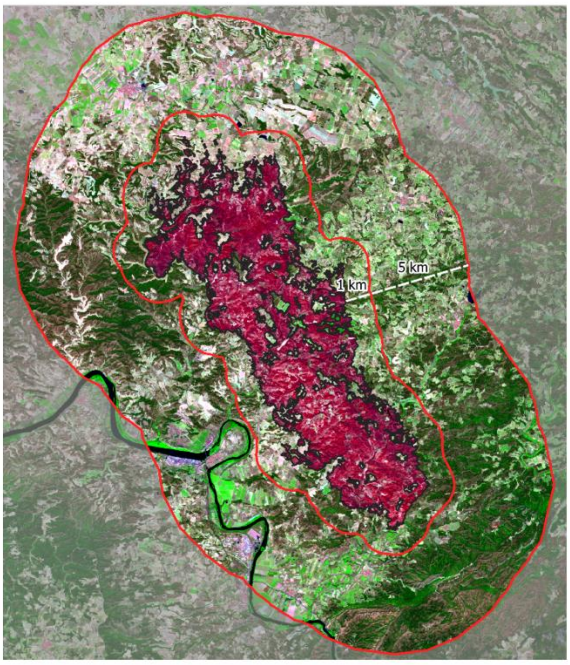

Figure 17 Schema of control zones 1 and 2 for the Torre de l'Espanyol wildfire. Background: Sentinel-2 RGB composition (Red: SWIR, Green: NIR and Blue: Red band)

As shown in the graphs (Figure 18 and Figure 19), the index time-series in a Mediterranean climate exhibits a clear seasonal pattern, with vegetation vigour and growth rates peaking in winter and reaching their lowest points in summer. In these graphics, three lines represent the behaviour of different areas: the burned zones (in blue), control zone 1 (in orange), and control zone 2 (in green). Similar to Figure 15 and Figure 16, the wildfire event's impact is distinctly visible. However, other patterns, such as the persistent drought (2021-2024), also emerge; this is evident in the control zones, where a downward linear trend indicates the ongoing effects of drought stress on vegetation outside the burned area.

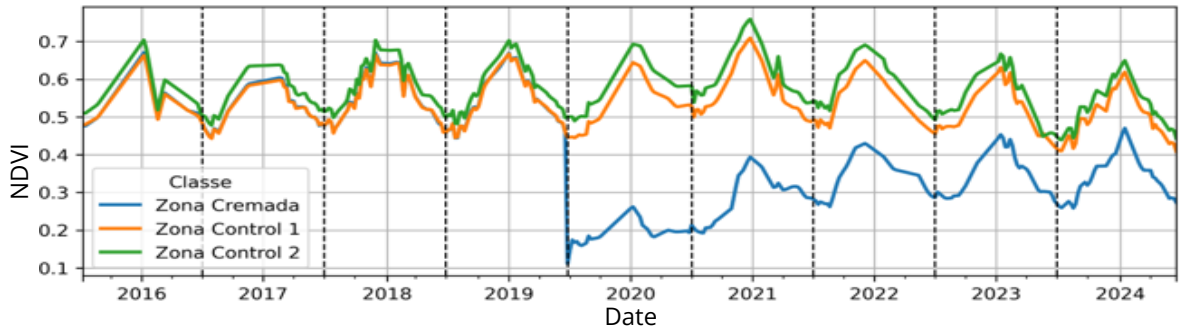

Figure 18 NDVI evolution from 2015 to 2024. Dashed lines represent 30th June of each year

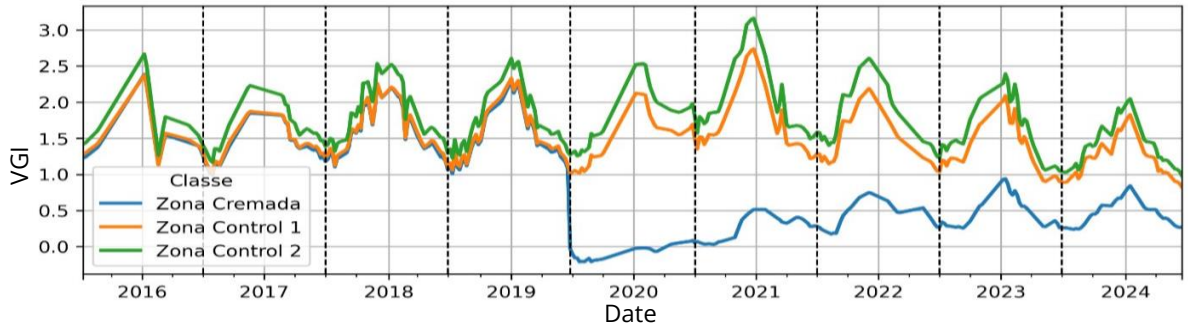

Figure 19 VGI evolution from 2015 to 2024. Dashed lines represent 30th June of each year

To assess the recovery of the burned area compared to the control zones, we analyse the difference in their time series. Initially, in the years directly following the wildfire, the burned area shows minimal response in these indices, reflecting the significant impact of the fire. However, after 3-4 years, the dynamics of the burned area increasingly resemble those of the control zones, with seasonal effects and trends aligning more closely. This convergence can be quantified by analysing the slope of the difference between the burned area and control zones (marked in red in the Figure 20). When the derivative of this difference function approaches zero, it indicates that the patterns are nearly identical, varying primarily in scale and absolute values.

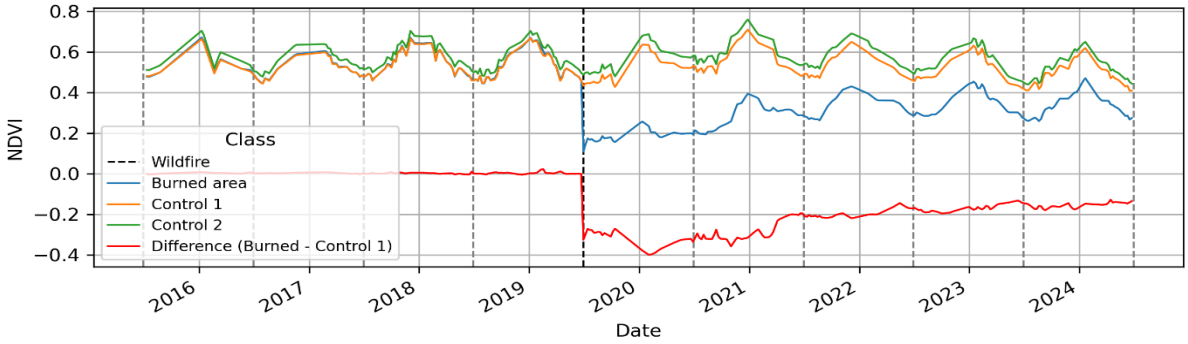

Figure 20 NDVI evolution with the representation of the difference between burned areas and control zone 1

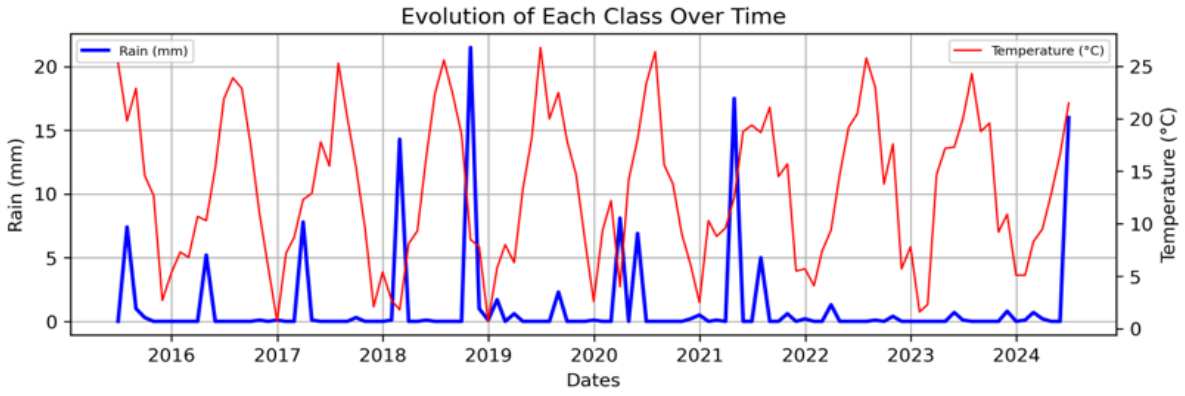

Figure 21 Weather data of monthly aggregated precipitation (blue) and average temperature (red) in the Torre de l'Espanyol region

Finally, to further refine the characterization of the forest masses, we incorporate weather data as additional inputs. After conducting a correlation analysis, we identified temperature, precipitation and humidity as the most representative variables for influencing vegetation dynamics. The graph in Figure 21 illustrates two of these variables and it helped confirm the inferences drawn from the index time-series analysis, particularly regarding the drought. Notably, the weather data reveals a significant dry period from 2021 to 2024, which is consistent with the downward trend observed in the control zones and reinforces the impact of the prolonged drought on vegetation growth.

3.5 ISS Implementation

In the motive of making the data accessible and exploitable one of the compromises of this Innovative Action is to aggregate all the analysed data in a Geo-Service. Technosylva, partners and coordinators of WP5 have developed a platform called Integrative Software System (ISS) to visualize and interact with the data generated in various IAs. In the case of the IA 5.3, the module allows for the visualization of the different indexes per each analysed wildfire and has a slider bar to change the date of the data, as shown in Figure 22.

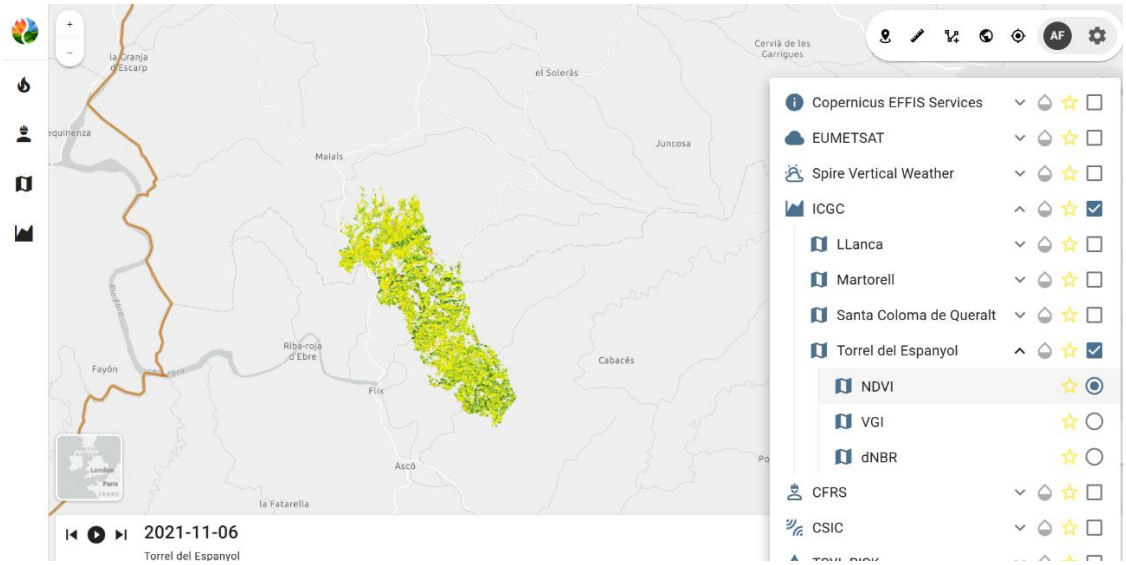

Figure 22 Screenshot of ISS platform showing the 6th November 2021 NDVI within the Torre de l'Espanyol fire, the dropdown menu at the right and the date slider bar at the bottom

Other capabilities of the module are the precise time-series generator, which originates the time-series of the desired area for all the indexes (Figure 23). And finally, detailed tables with the CO_2 emissions and the burned biomass for each wildfire (Figure 24).

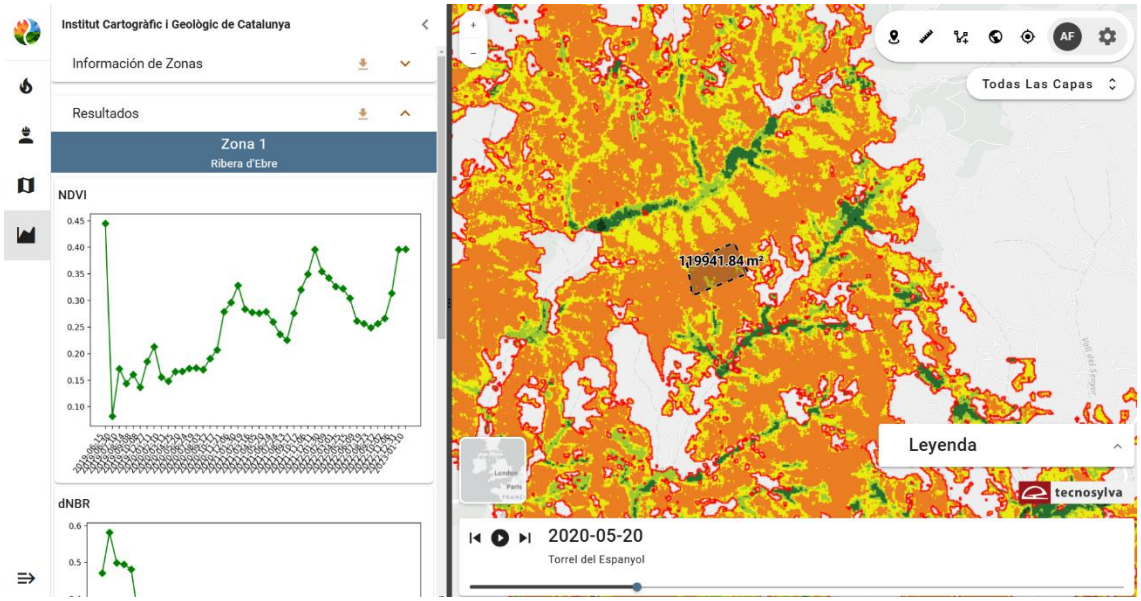

Figure 23 Screenshot of ISS time-series generator capabilities. The area is drawn in the map and the desired time-series graph appears on the left of the screen

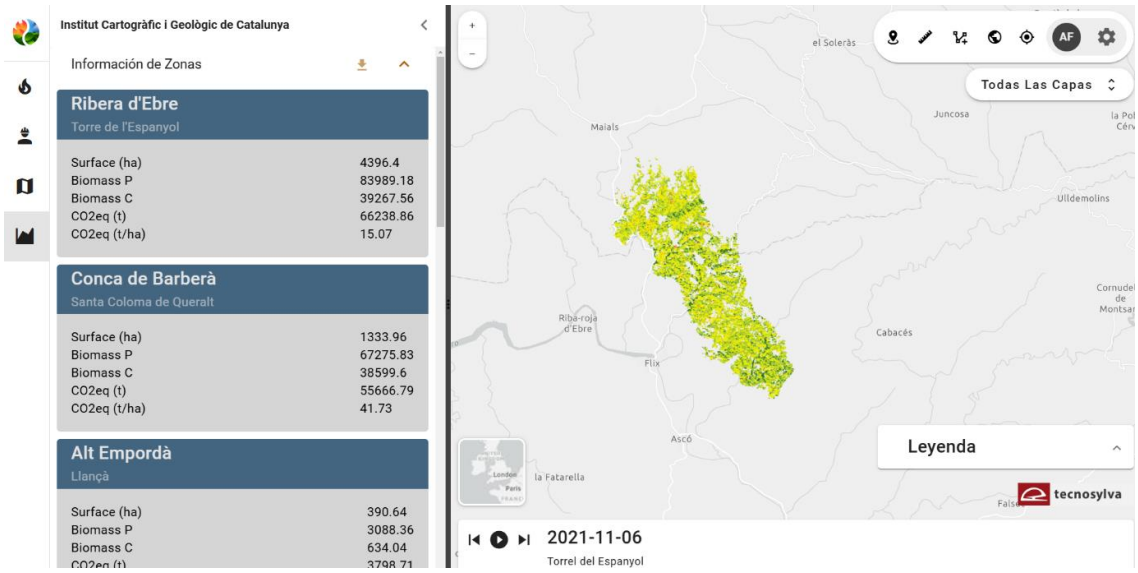

Figure 24 Screenshot of ISS with the information of the CO_2 emissions and burned biomass per wildfire

4. Technology Readiness

Technology Readiness Levels (TRL) are a standardized scale used to assess the maturity of a particular technology during its development and deployment (European Commission, 2014). The scale ranges from TRL1 (basic principles observed) to TRL9 (actual system proven in operational environment). The following definitions apply:

TRL 1 – basic principles observed
TRL 2 – technology concept formulated
TRL 3 – experimental proof of concept
TRL 4 – technology validated in lab
TRL 5 – technology validated in relevant environment
TRL 6 – technology demonstrated in relevant environment
TRL 7 – system prototype demonstration in operational environment
TRL 8 – system complete and qualified
TRL 9 – actual system proven in operational environment

This section will assess the Technical Readiness Levels that are achieved in relation to the main results of this deliverable.

4.1. Atmospheric Data Collection

The development work described in Part 1 of this report focuses on leveraging satellite-based Radio Occultation data for atmospheric profiling and its integration into Numerical Weather Prediction models to enhance wildfire resilience.

Based on the activities detailed in this report, a fully operational and qualified system for leveraging Radio Occultation technology, Data Assimilation, and Numerical Weather Prediction (NWP) systems to enhance extreme wildfire resilience is in place. Hence, the technology can be assessed at TRL 8. The system provides accurate, real-time atmospheric insights critical for assessing wildfire risks. Achieving TRL 8 signifies that the technology has been thoroughly tested, validated, and proven effective. This level of maturity is vital because it ensures that the technology can reliably support decision-making processes in real-world applications, enabling proactive fire management and more effective resource allocation during extreme wildfire events.

4.2 Vegetation Data Collection

The work conducted in the IA 5.3 began at Technology Readiness Level (TRL) 6, involving the development of methodologies that were applied to real-world wildfire scenarios. These methodologies, integrating various types of Earth observation data and Artificial Intelligence, have been successfully implemented via an API into the ISS software, a web-

based geo platform developed by Technosylva. This successful integration allows for the visualisation, consultation, and downloading of the analysed data. As a result, the project will advance to TRL 8, signifying that the system is now complete and qualified.

5. CONCLUSIONS

Part 1 of this report highlights the significant advancements achieved by leveraging Spire's satellite-based Radio Occultation (RO) technology to enhance atmospheric profiling and improve Numerical Weather Prediction models.

Spire's constellation of nanosatellites collects unbiased and globally distributed RO profiles with high vertical resolution, offering a valuable dataset for refining forecast accuracy in wildfire-prone regions. By utilizing a hybrid 4DEnVar assimilation technique, Spire has successfully integrated RO data into its global forecast models, providing actionable insights into critical atmospheric variables such as temperature, humidity, and wind patterns. These improvements enhance the ability to predict wildfire risks, enabling more proactive and efficient fire management strategies.

The results demonstrate that Spire's RO data and forecasting systems have reached Technology Readiness Level (TRL) 8, signifying a complete and qualified system ready for operational deployment. By providing accurate, real-time atmospheric data, a significant step toward building a more resilient wildfire management system across Europe has been taken. Moving forward, the continued operational use and refinement of this technology will further enhance its capacity to support decision-makers in preventing and combating wildfires.

As final remarks for part 2, successfully estimating CO_2 emissions released in wildfires using only free-access Earth observation (EO) data can be crucial for initial assessments of wildfire impacts and comprehensive wildfire analyses. This method allows for prompt estimations of emissions across the entire affected area, providing timely information while on-ground analyses are being conducted or when they cannot be performed.

One of the strengths of this approach is its worldwide applicability. However, the current methodologies do have some limitations. To deploy this analysis for any wildfire globally, it is essential to identify EO sources equivalent to those used in this study and to adapt the coefficients in the methodologies as necessary.

Additionally, incorporating Artificial Intelligence can produce novel approaches to post-fire forest recovery assessments by analysing large and diverse data sources more efficiently, leading to better characterisation and modelling of recovery processes. This will enhance the analysis capabilities and the understanding of the factors that intervene in these processes, from an EO standpoint.

Finally, the integration of platforms like Technosylva's ISS is transforming the way we approach and understand complex challenges. By seamlessly aggregating diverse datasets and delivering rapid, reliable access to critical information, this technology addresses a growing demand among private and public stakeholders. Its ability to streamline decision-making and enhance situational awareness makes it an indispensable tool for driving smarter, more effective solutions.

6.REFERENCES

Anthes, R. A., Bernhardt, P. A., Chen, Y., Cucurull, L., Dymond, K. F., Ector, D., Healy, S. B., Ho, S.-P., Hunt, D. C., Kuo, Y.-H., Liu, H., Manning, K., McCormick, C., Meehan, T., Randel, W. J., Rocken, C., Schreiner, W. S., Sokolovskiy, S. V., Syndergaard, S., Thompson, D. C., Trenberth, K. E., Wee, T.-K., Yen, N. L., & Zeng, Z. (2008). The COSMIC/FORMOSAT-3 mission: Early results. *Bulletin of the American Meteorological Society*, 89(3), 313-334.

Bauer, P., Radnoti, G., Healy, S., & Cardinali, C. (2014). GNSS radio occultation observing system experiments. *Monthly Weather Review*, 142, 555-572.

Bowler, N. (2020). An assessment of GNSS radio occultation data produced by Spire. *Quarterly Journal of the Royal Meteorological Society*, 146(733), 3772-3788.

Cappaert, J. (2018). Building, deploying and operating a cubesat constellation – exploring the less obvious reasons space is hard, SSC18-IV-03. In: *Proceedings of the AIAA/USU Conference on Small Satellites* – Delivering Mission Success

Cardinali, C., 2009. Monitoring the observation impact on the short-range forecast. *Quarterly Journal of the Royal Meteorological Society*, 135, 239-250. https://doi.org/10.1002/qj.366.

Cardinali, C, Healy, S. (2011). GPS-RO at ECMWF. In: *Proceedings of the Seminar on data assimilation for atmosphere and ocean of the European Centre for Medium Range Weather Forecasts*. Reading, United Kingdom, p. 323-36.

Cardinali, C. & Healy, S. (2014). Impact of GPS radio occultation measurements in the ECMWF system using adjoint-based diagnostics. *Quarterly Journal of the Royal Meteorological Society*, 140, 2315-2320.

Cucurull, L., Derber, J. C., Treadon, R., and Purser, R. J. (2008). Preliminary impact studies using Global Positioning System radio occultation profiles at NCEP. *Monthly Weather Review*, 136, 1865-1877.

Cucurull, L. (2010). Improvement in the use of an operational constellation of GPS radio occultation receivers in weather forecasting. *Weather and Forecasting*, 25(2), 749-767.

De Santis, A., Asner, G. P., Vaughan, P. J., & Knapp, D. E. (2010). Mapping burn severity and burning efficiency in California using simulation models and Landsat imagery. *Remote Sensing of Environment, 114*(7), 1535-1545. https://doi.org/10.1016/j.rse.2010.02.010

Desroziers, Gérald, et al (2005). "Diagnosis of observation, background and analysis-error statistics in observation space." *Quarterly Journal of the Royal Meteorological Society,* 131.613: 3385-3396.

European Commission (2014). Technology Readiness Levels (TRL): Horizon 2020 Work Programme 2014-2015 General Annexes. *European Commission*. Retrieved from

https://ec.europa.eu/research/participants/data/ref/h2020/wp/2014_2015/annexes/h2020-wp1415-annex-g-trl_en.pdf.

Feliu Serra-Burriel, P., Delicado, P., Prata, A. T., & Cucchietti, F. M. (2021). Estimating heterogeneous wildfire effects using synthetic controls and satellite remote sensing. *Remote Sensing of Environment, 265*, 112649. https://doi.org/10.1016/j.rse.2021.112649

Gorbunov, M., Irisov, V., & Rocken, C. (2022). Noise floor and signal-to-noise ratio of radio occultation observations: a cross-mission statistical comparison. *Remote Sensing*, 14(3), 691.

Harnisch, F., Healy, S., Bauer, P., & English, S. (2013). Scaling of GNSS Radio Occultation impact with observation number using an Ensemble of Data Assimilations. *Monthly Weather Review*, 141, 4395-4413.

Harris, L., and S. Lin (2013). A two-way nested global-regional dynamical core on the cubed-sphere grid. *Monthly Weather Review*, 141, 283–306, https://doi.org/10.1175/MWR-D-11-00201.1.

Healy, S. B. (2020). 2020 - a crazy year (for satellite navigation and NWP). *ECMWF Science Blog* (available at https://www.ecmwf.int/en/about/media-centre/science-blog/2020/2020-crazy-year-satellite-navigation-data-and-nwp).

Ho, S. P., Anthes, R. A., Ao, C. O., Healy, S., Horanyi, A., Hunt, D., Mannucci, A. J., Pedatella, N., Randel, W. J., Simmons, A., Steiner, A., Xie, F., Yue, X. & Zeng, Z. (2020). The COSMIC/FORMOSAT-3 radio occultation mission after 12 years: Accomplishments, remaining challenges, and potential impacts of COSMIC-2. *Bulletin of the American Meteorological Society*, 101(7), E1107-E1136.

Ho, S. P., Kireev, S., Shao, X., Zhou, X., & Jing, X. (2022). Processing and validation of the STAR COSMIC-2 temperature and water vapor profiles in the neutral atmosphere. *Remote Sensing*, 14(21), 5588.

Ho, S. P., Zhou, X., Shao, X., Chen, Y., Jing, X., & Miller, W. (2023). Using the commercial GNSS RO spire data in the neutral atmosphere for climate and weather prediction studies. *Remote Sensing*, 15(19), 4836.

Jing, X., Ho, S. P., Shao, X., Liu, T. C., Chen, Y., & Zhou, X. (2023). Spire RO Thermal Profiles for Climate Studies: Initial Comparisons of the Measurements from Spire, NOAA-20 ATMS, Radiosonde, and COSMIC-2. *Remote Sensing*, 15(15), 3710.

Key, C. H., & Benson, N. C. (2005). Landscape assessment: ground measure of severity, the composite burn index; and remote sensing of severity, the normalized burn ratio. *FIREMON: Fire effects monitoring and inventory system, 2004*. https://doi.org/10.2737/RMRS-GTR-164-CD

Kleist, D. T., & Ide, K. (2015). An OSSE-based evaluation of hybrid variational–ensemble data assimilation for the NCEP GFS. Part II: 4DEnVar and hybrid variants. *Monthly Weather Review*, 143(2), 452–470. https://doi.org/10.1175/MWR-D-13-00350.1.

Lackner, B. C., Steiner, A. K., Hegerl, G. C., & Kirchengast, G. (2011). Atmospheric climate change detection by radio occultation data using a fingerprinting method. *Journal of climate*, *24*(20), 5275-5291.

Langland R. and N.L Baker (2004). Estimation of observation impact using the NRL atmospheric variational data assimilation adjoint system. *Tellus*, 56A, 189-201.

Lonitz, K. Bowler, N. Holm, E. & Healy, S. (2021). Assimilating Spire and COSMIC-2 data into the IFS. *ECMWF Newsletter* #169, 25-32.

Marshall, J. L., Xiao, Y., Norman, R., Zhang, K., Rea, A., Cucurull, L., Seecamp, R., Steinle, P., Puri, K., Fu, E. & Le, T. (2012). The application of radio occultation observations for climate monitoring and numerical weather prediction in the Australian region. *Australian Meteorological and Oceanographic Journal*, 62, 323-334.

McCarty, W., Patrick, O., Damon, M. R., & Hall, A. A. (2021). Science utilizing data from spire global as part of the NASA commercial Smallsat data acquisition program. In *2021 IEEE International Geoscience and Remote Sensing Symposium* IGARSS (pp. 604-607). IEEE.

Montero, G., Pasalodos-Tato, M., López-Senespleda, E., Onrubia, R., & Madrigal, G. (2013). Ecuaciones para la estimación de la biomasa en matorrales y arbustedos mediterráneos. *6CFE01-139*.

Qiu, C., Wang, X., Zhou, K., Zhang, J., Chen, Y., Li, H., Liu, D. & Yuan, H. (2023). Comparative Assessment of Spire and COSMIC-2 Radio Occultation Data Quality. *Remote Sensing*, 15(21), 5082.

Rocken, C., Anthes, R., Exner, M., Hunt, D., Sokolovskiy, S., Ware, R., Gorbunov, M., Schreiner, W., Feng, D., Herman, B., Kuo, Y.-H. & Zou, X. (1997). Analysis and validation of GPS/MET data in the neutral atmosphere. *Journal of Geophysical Research: Atmospheres,* 102(D25), 29849-29866.

Saulino, L., Rita, A., Migliozzi, A., Maffei, C., Allevato, E., Garonna, A. P., & Saracino, A. (2020). Detecting burn severity across Mediterranean forest types by coupling medium-spatial resolution satellite imagery and field data. *Remote Sensing, 12*(4), 741. https://doi.org/10.3390/rs12040741

Tardà Lleget, A. (2022). *Identificació i traçabilitat de les masses forestals al Massís del Montseny, a partir de l'anàlisi espectral de sèries temporals de dades d'Observació de la Terra* (Doctoral dissertation, Universitat de Barcelona). Universitat de Barcelona Digital Repository. http://hdl.handle.net/2445/191209

Turco, M., von Hardenberg, J., AghaKouchak, A., Llasat, M. C., Provenzale, A., & Trigo, R. M. (2017). On the key role of droughts in the dynamics of summer fires in Mediterranean Europe. *Scientific Reports, 7*(1), 1-10. https://doi.org/10.1038/s41598-017-00116-9

Weiss, J. (2022). COSMIC-2: Highlights from 3 Years in Orbit. Presented at *Joint OPAC-7 and IROWG-9*. Leibnitz, Austria. September 8, 2022. https://static.uni-graz.at/fileadmin/veranstaltungen/opacirowg2022/programme/08.9.22/AM/Session_2/OPAC-IROWG-2022_Weiss.pdf

Wickert, J., G. Beyerle, R. König, S. Heise, L. Grunwaldt, G. Michalak, C. Reigber, and T. Schmidt (2005). GPS radio occultation with CHAMP and GRACE: A first look at a new and promising satellite configuration for global atmospheric sounding. *Ann. Geophys.*, 23, 653–658, https://doi.org/10.5194/angeo-23-653-2005.

Wiedinmyer, C., Quayle, B., Geron, C., Belote, A., McKenzie, D., Zhang, X., & Wynne, K. K. (2006). Estimating emissions from fires in North America for air quality modeling. *Atmospheric Environment, 40*(19), 3419-3432. https://doi.org/10.1016/j.atmosenv.2006.02.010

Commercial Weather Data Pilot (CWDP) Round 2 Summary (2020)

Quality Assessment of Commercial GNSS-RO Data (2020)

FIRE-RES